The Impact of Dilatation, Scrambling and Pressure Transport in Turbulent Premixed Flames

Lu Tian[a] and Rune Peter Lindstedt[a]*

[a]*Department of Mechanical Engineering, Imperial College, Exhibition Road, London SW7 2AZ, UK*

(*Received 00 Month 200x; final version received 00 Month 200x*)

Premixed turbulent flames feature strong interactions between chemical reactions and turbulence that affect scalar and turbulence statistics. The focus of the present work is on clarifying the impact of pressure dilatation/flamelet scrambling effects with a comprehensive second–moment closure used for evaluation purposes. Model extensions that take into account flamelet orientation and molecular diffusion are derived. Isothermal pressure transport is included with an additional variable density contribution derived for the flamelet regime of combustion. The full closure is assessed by comparisons with direct numerical simulations (DNS) of statistically “steady" fully developed premixed turbulent planar flames at different expansion ratios. Subsequently, the prediction of lean premixed turbulent methane–air flames featuring fractal grid generated turbulence in an opposed jet geometry is considered. The overall agreement shows that “dilatation" effects contribute to counter–gradient transport and can also increase the turbulent kinetic energy significantly. Levels of anisotropy are broadly consistent with the DNS data and key aspects of opposed jet flames are well predicted. However, it is also shown that complications arise due to interactions between the imposed pressure gradient and combustion and that redistribution is affected along with the scalar flux at the leading edge. The latter is strongly affected by the reaction rate closure and, potentially, by pressure transport. Overall, the derived models offer significant improvements and can readily be applied to the modelling of premixed turbulent flames at practical rates of heat release.

Keywords: second-moment closure; variable density effects; dilatation model; opposed jets; premixed turbulent flames

1. Introduction

Modelling of premixed turbulent flames has the potential to provide guidance for industrial applications, such as burners, gas turbines, internal combustion engines and the assessment of large-scale explosions at industrial plants [1]. Such flames usually feature large physical domains and high Reynolds numbers that preclude the use of Direct Numerical Simulations. Large Eddy Simulations (LES), which resolve large-scale turbulent motions, can present an attractive alternative [2]. However, chemical reactions typically occur on the unresolved scales and correlations with pressure fluctuations can result in significant cross–scale (i.e. backscatter) energy transfer [3]. The current study investigates the modelling of related correlations using moment based methods that offer a partial resolution of the unsteady fluid motion [4]. The main task for such methods remains the closure of Reynolds stresses, turbulent scalar fluxes and the mean reaction rate. Numerous studies of premixed turbulent flames [5–11] have concentrated on the closure of the mean reaction rate in the flamelet combustion regime and beyond. Sabelnikov et al. [11] recently proposed a direct transport equation for the mean reaction rate and the modelling of two dominant source terms that highlight the influence of turbulent stretching on the mean reaction rate. However, the impact of chemical reaction on turbulence has attracted

*Corresponding author. Email: p.lindstedt@imperial.ac.uk

less attention. Experimental [12–14] and direct numerical simulation (DNS) [3, 15–19] studies reveal that variable density effects induced by combustion are significant. Such effects are associated with mean pressure gradient and fluctuating velocity/scalar – pressure gradient correlations. The former can be explicitly transformed into known quantities through the application of Bray–Moss–Libby (BML) theory (e.g. [1, 20]); the latter also affect anisotropy via combustion–induced expansion and pressure fluctuations.

Past analyses of DNS data confirm that redistribution and dilatation terms largely outweigh other contributions [15, 21, 22]. Similarly, the importance of the scrambling term is confirmed based on the analysis of the scalar–flux transport equation [18, 23–25]. Recent analysis of DNS databases [3] using a differential filter suggests that the modelling of the pressure gradient – velocity correlation is important in Large-Eddy Simulations (LES) as combustion–induced subgrid-scale thermal expansion leads to substantial cross–scale energy transfer. The common way of accounting for the effects of combustion on pressure redistribution/scrambling terms is a density–weighted rewriting of second–moment models derived on a constant density basis [26–28]. However, a number of studies showed that such an approach is insufficient for premixed turbulent flames [29–31]. Bailly et al. [29] and Karmed et al. [30] invoked a closure via an additional mean pressure gradient term. Lindstedt and Váos [31] modelled redistribution/scrambling and dissipation terms together by decomposing the closure into density–weighted and preferential acceleration parts. The latter was obtained from a second–order Isotropisation of Production (IP) type model [32]. Nevertheless, pressure dilatation and flame–generated pressure scrambling (flamelet scrambling) models have seldom been included into second–moment transport equations due to implementation difficulties. However, it has been shown by Robin et al. [33] that flame generated “dilatation" effects can be significant and may outweigh other pressure related effects.

The importance of pressure related dilatation was arguably first pointed out by Kuznetsov [34] with the flame–front contribution analysed. The derived expression was related to the completeness of combustion and laminar flame properties. The expression was not closed due to the lack of data on pressure pulsations conditioned at the flame front. Zhang and Rutland [21] proposed an expression for the conditional pressure fluctuation based on their DNS data. The resulting model has the advantage of contributing a positive effect throughout the flame brush. However, the closure is partially inconsistent with the commonly adopted BML theory as the conditional pressure fluctuation does not vanish at the leading edge of a flame [35]. Hůlek and Lindstedt [36] suggested a different expression for the conditional pressure fluctuation that implies zero-pressure rise ahead of the flame front. The resulting closure for the dilatation term is consistent with the thermochemistry applied and limits “dilatation" effects to within the flame brush. Domingo and Bray [35] closed the fluctuating velocity/scalar – pressure gradient correlations by separately considering the contributions of reactant, flame and product zones. The derivation was, in general, consistent with the aforementioned study by Hůlek and Lindstedt [36]. It is also noted that the pressure dilatation term can also be derived from the instantaneous continuity and scalar equations and the linear relationship between reaction progress variable and specific volume [31]. The resulting expression consists of two parts associated with molecular diffusion and reaction–rate correlation effects. The former is typically neglected [21, 25, 35, 36] on the basis of a dimensional analysis [37]. However, the associated second derivative can be significant for premixed turbulent flames. The value of molecular diffusivity is significantly boosted in high–temperature flame regions and the impact has been explored using Reynolds–Averaged Navier–Stokes equations (RANS) and LES of premixed turbulent flames [38, 39]. The studies indicate that the effects of molecular diffusion should be included in the modelling of pressure dilatation and flamelet scrambling. In addition, DNS studies [15, 17] suggest that pressure transport can be as important as dilatation in premixed turbulent flames.

The treatment of turbulent kinetic energy dissipation (ϵ) also merits attention. The "standard" turbulent dissipation rate equation is based on the $k-\epsilon$ model [40] formulated for constant–density flows. However, Mura and Champion [41] found that beyond a given value of the Bray number, the turbulent dissipation rate may be controlled by the flamelet structures. Contributions from the mean pressure gradients have successfully been included in the turbulent dissipation rate equation [31, 42–45]. In addition, a renormalisation group (RNG) modification to the dissipation equation has been proposed by Yakhot et al. [46]. The additional strain-rate terms provide a slightly better agreement with experimental data in opposed jet flows [47, 48].

The main purpose of the present work is to derive, apply and assess dilatation/flamelet scrambling models associated with flame generated variable density effects. The opposed jet geometry features a strong imposed pressure gradient near the stagnation plane, while for freely propagating flames the pressure is reduced through the flame brush due to flow acceleration. The performance of the derived dilatation/flamelet scrambling models is thus evaluated in the presence of normal pressure gradients with opposite signs. The models include the flamelet orientation and the impact of molecular diffusion. Pressure transport is also included via a combination of isothermal [49] and flamelet contributions. The derivation of the latter is consistent with that of pressure dilatation/scrambling models. The complete closure is applied to flames in the flamelet regime of combustion [50].

2. Governing Equations

The present study investigates premixed turbulent incompressible flames with the assumptions of low Mach, high Reynolds, large Damköhler and unity Lewis numbers. The thermochemistry applied in the current work is consistent with the BML theory [1] with the averaged density obtained from the customary algebraic expression $\bar{\rho}=\frac{\rho_u}{1+\tau\widetilde{c}}$, where τ represents the expansion ratio between the unburnt and burnt gases, given by $\tau=\frac{\rho_u}{\rho_b}-1$, and $\widetilde{c}$ is the mean reaction progress variable. The aerothermochemical field is governed by the following Favre–averaged equations,

$$\frac{\partial\bar{\rho}}{\partial t}+\frac{\partial\bar{\rho}\widetilde{u_l}}{\partial x_l}=0 \tag{1}$$

$$\frac{\partial\bar{\rho}\widetilde{u_i}}{\partial t}+\frac{\partial\bar{\rho}\widetilde{u_l}\widetilde{u_i}}{\partial x_l}=-\frac{\partial\bar{p}}{\partial x_i}+\frac{\partial}{\partial x_l}(\overline{\tau_{il}}-\bar{\rho}\widetilde{u_i''u_l''}) \tag{2}$$

$$\frac{\partial\bar{\rho}\widetilde{c}}{\partial t}+\frac{\partial\bar{\rho}\widetilde{u_l}\widetilde{c}}{\partial x_l}=\frac{\partial}{\partial x_l}(\overline{j_l}-\bar{\rho}\widetilde{u_l''c''})+\overline{S_c} \tag{3}$$

where $\overline{\tau_{il}}=\overline{\mu_L(\frac{\partial u_i}{\partial x_l}+\frac{\partial u_l}{\partial x_i}-\frac{2}{3}\delta_{il}\frac{\partial u_k}{\partial x_k})}$ and $\overline{j_l}=\overline{\rho D_c\frac{\partial c}{\partial x_l}}$ represent the molecular viscous stress tensor and diffusion flux vector. The dynamic viscosity is obtained from the power-law expression $\mu_L=\mu_{ref}(\frac{\widetilde{T}}{\widetilde{T}_{ref}})^{\frac{2}{3}}$ [51], where μ_{ref} is the value at $\widetilde{T}_{ref}$ $(=298.15$ K). The mass diffusivity D_c is calculated using a constant Schmidt number of 0.7.

The unclosed terms for the above equations are Reynolds stresses ($\widetilde{u_i''u_l''}$), scalar fluxes ($\widetilde{u_l''c''}$) and the chemical reaction source term ($\overline{S_c}$). In the framework of second–moment

closures, Reynolds stresses and scalar fluxes can be modelled by their transport equations,

$$\frac{\partial \bar{\rho}\widetilde{u_i''u_j''}}{\partial t} + \frac{\partial \bar{\rho}\widetilde{u}_l\widetilde{u_i''u_j''}}{\partial x_l} = -\frac{\partial \bar{\rho}\widetilde{u_i''u_j''u_l''}}{\partial x_l} - \bar{\rho}\left(\widetilde{u_i''u_l''}\frac{\partial \widetilde{u}_j}{\partial x_l} + \widetilde{u_j''u_l''}\frac{\partial \widetilde{u}_i}{\partial x_l}\right) - \left[\overline{u_i''}\frac{\partial \bar{p}}{\partial x_j} + \overline{u_j''}\frac{\partial \bar{p}}{\partial x_i}\right] - \left[\overline{u_i''\frac{\partial p'}{\partial x_j}} + \overline{u_j''\frac{\partial p'}{\partial x_i}}\right] - \left[\overline{\tau_{il}\frac{\partial u_j''}{\partial x_l}} + \overline{\tau_{jl}\frac{\partial u_i''}{\partial x_l}}\right] \tag{4}$$

The right hand side of Eq. (4) includes (in order) terms for the transport of Reynolds stresses, the production by mean strain and mean pressure gradients, fluctuating velocity – pressure gradient correlation and viscous dissipation.

$$\frac{\partial \bar{\rho}\widetilde{u_i''c''}}{\partial t} + \frac{\partial \bar{\rho}\widetilde{u}_l\widetilde{u_i''c''}}{\partial x_l} = -\frac{\partial \bar{\rho}\widetilde{u_i''u_j''c''}}{\partial x_l} - \bar{\rho}\left(\widetilde{u_l''c''}\frac{\partial \widetilde{u}_i}{\partial x_l} + \widetilde{u_i''u_l''}\frac{\partial \widetilde{c}}{\partial x_l}\right) - \overline{c''}\frac{\partial \bar{p}}{\partial x_i} - \overline{c''\frac{\partial p'}{\partial x_i}} + \overline{u_i''S_c} - \left[\overline{\tau_{il}\frac{\partial c''}{\partial x_l}} + \overline{j_l\frac{\partial u_i''}{\partial x_l}}\right] \tag{5}$$

Similarly, the right hand side of Eq. (5) includes (in order) terms for the turbulent transport of scalar fluxes, the production by mean strain and mean scalar gradients, mean pressure gradients, fluctuating scalar – pressure gradient correlation, turbulence – reaction rate correlation and viscous dissipation. The production terms are exact with other terms requiring modelling. In particular, BML theory provides the time–averaged density–weighted velocity and scalar fluctuations ($\overline{u_i''}$ and $\overline{c''}$) given in Eqs. (6) and (7). The conversion from Reynolds to Favre–averages for other presumed *pdf* shapes may be derived based on the study by Kolla and Swaminathan [52].

$$\overline{u_i''} = \tau\frac{\bar{\rho}}{\rho_u}\widetilde{u_i''c''} \tag{6}$$

$$\overline{c''} = \tau\frac{\bar{\rho}}{\rho_u}\widetilde{c''^2} \tag{7}$$

The ϕ_{ij} and ϕ_{ic} terms arguably mark the most problematic part of turbulence closures. For modelling proposes, the former is rewritten as anisotropic and isotropic parts. The redistribution term forms the anisotropic part of the fluctuating velocity – pressure gradient correlation in the Reynolds–stress transport equation,

$$\phi_{ij}^R = -\left[\overline{u_i''\frac{\partial p'}{\partial x_j}} + \overline{u_j''\frac{\partial p'}{\partial x_i}} - \frac{2}{3}\delta_{ij}\overline{u_l''\frac{\partial p'}{\partial x_l}}\right] \tag{8}$$

The isotropic part is further separated into pressure transport and dilatation terms.

$$\phi_{ij}^T = -\frac{2}{3}\delta_{ij}\overline{\frac{\partial p'u_l''}{\partial x_l}} \tag{9}$$

$$\phi_{ij}^D = \frac{2}{3}\delta_{ij}\overline{p'\frac{\partial u_l''}{\partial x_l}} \tag{10}$$

The fluctuating scalar – pressure gradient correlation (ϕ_{ic}) in the scalar–flux transport equation can accordingly be separated into pressure transport and “scrambling" terms,

$$\phi_{ic}^{T} = -\overline{\frac{\partial p' c''}{\partial x_l}} \tag{11}$$

$$\phi_{ic}^{S} = \overline{p' \frac{\partial c''}{\partial x_l}} \tag{12}$$

The pressure transport terms, usually neglected in past studies, are included along with the pressure dilatation/flamelet scrambling contributions as discussed below.

3. Extended Treatment of Variable Density Effects

Variable density effects in premixed turbulent flames include mean pressure gradient induced preferential acceleration effects and volume expansion. The derivation of the new dilatation/flamelet scrambling models is presented in Section 3.1 and the corresponding flamelet pressure transport model is in Section 3.2 (also see Appendices A and B). The preferential acceleration effects [31] are introduced in Section 3.3 as the impact of volume expansion is significant in the flamelet regime of combustion (e.g. [33, 36, 41]).

3.1 *Dilatation and Scrambling Terms*

Expansion due to combustion within flamelets is a major contributor to dilatation effects and the volume average of pressure dilatation and flamelet scrambling terms can be transformed into a flame surface average in the manner of Zhang and Rutland [21],

$$\overline{p' \frac{\partial u_i''}{\partial x_i}} = \frac{1}{V} \int_V p' \frac{\partial u_i''}{\partial x_i} \mathrm{d}V = \Sigma \Big\langle \int_\xi p' \frac{\partial u_i''}{\partial x_i} \mathrm{d}\xi \Big\rangle_s \tag{13}$$

$$\left(\overline{p' \frac{\partial c''}{\partial x_i}} \right)_f = \frac{1}{V} \int_V p' \frac{\partial c''}{\partial x_i} \mathrm{d}V = \Sigma \Big\langle \int_\xi p' \frac{\partial c''}{\partial x_i} \mathrm{d}\xi \Big\rangle_s \tag{14}$$

where ξ is the axis normal to local flame pointing to products and x_i is the coordinate system for flow field, as illustrated in Fig. 1. The subscript f indicates the flame contribution, S the flame surface area within the volume V; $<>_s$ a flame surface average and $\Sigma = \frac{S}{V}$ the flame surface density, related to the chemical reaction rate ($\overline{S_c} = \rho_u S_L \Sigma$). Consistent with the flamelet approximation, it is assumed that turbulence does not (strongly) affect chemical reactions within flamelets. The following relations can be obtained using the one–dimensional momentum equation [21, 53],

$$\overline{p' \frac{\partial u_i''}{\partial x_i}} = \overline{S_c} (\tau S_L)^2 \Big(\frac{< p_u - \overline{p} >_s}{\triangle p} - \frac{1}{2} \Big) \big\langle \big(\boldsymbol{n} \cdot \boldsymbol{N_i} \big) \big(\boldsymbol{n} \cdot \boldsymbol{N_i} \big) \big\rangle \tag{15}$$

$$\left(\overline{p' \frac{\partial c''}{\partial x_i}} \right)_f = \overline{S_c} (\tau S_L) \Big(\frac{< p_u - \overline{p} >_s}{\triangle p} - \frac{1}{2} \Big) \big\langle \boldsymbol{n} \cdot \boldsymbol{N_i} \big\rangle \tag{16}$$

$$\triangle p = \rho_u S_L^2 \tau$$

The flamelet orientation angle, c.f. DNS [35, 54] and experimental [55, 56] studies, is included with $\boldsymbol{n}$ the unit vector ξ pointing from reactants to products and $\boldsymbol{N_i}$ the unit

vector of x_i and $\triangle p$ represents the pressure drop across flamelets. The surface average of the pressure difference at the flame leading edge $< p_u - \overline{p} >_s$ (see Eq. (15)) has been discussed elsewhere [31, 35] and the current work is using the form below [36].

$$< p_u - \overline{p} >_s = \bar{c}\triangle p \tag{17}$$

An alternative [21] expression $< p_u - \overline{p} >_s = (1 + \widetilde{c})\triangle p/2$ appears less satisfying in that the conditional pressure difference does not vanish at the leading edge of the flame [35]. Nishiki et al. [17] circumvented the issue by simply scaling p' with the laminar pressure drop $p' \sim \triangle p = \rho_u S_L^2 \tau$ [17]. Substitution of Eq. (17) into Eqs. (15)-(16) gives,

$$\overline{p' \frac{\partial u_i''}{\partial x_i}} = \overline{S_c}(\tau S_L)^2 \big(\bar{c} - \frac{1}{2}\big) \big\langle \big(\boldsymbol{n} \cdot \boldsymbol{N_i}\big)\big(\boldsymbol{n} \cdot \boldsymbol{N_i}\big) \big\rangle \tag{18}$$

$$\left(\overline{p' \frac{\partial c''}{\partial x_i}}\right)_f = \overline{S_c}(\tau S_L)\big(\bar{c} - \frac{1}{2}\big) \big\langle \boldsymbol{n} \cdot \boldsymbol{N_i} \big\rangle \tag{19}$$

The pressure dilatation term can also be derived from the instantaneous continuity and scalar equations and the linear relationship between the reaction progress variable (c) and specific volume ($1/\rho$),

$$\overline{p' \frac{\partial u_i''}{\partial x_i}} = \overline{p' \frac{\partial}{\partial x_i}\Big[\rho D_c \frac{\partial c''}{\partial x_i}\Big] \frac{\partial \rho^{-1}}{\partial c}} + \overline{p' S_c \frac{\partial \rho^{-1}}{\partial c}} \tag{20}$$

where D_c represents the molecular diffusion coefficient. The second term is equivalent to Eq. (18). The first term in Eq. (20) is commonly neglected on the basis of a dimensional analysis of diffusion flames [37]. However, it can be significant in premixed turbulent flames [38, 39, 57]. Mantel and Borghi [58] developed a transport equation based closure for the scalar dissipation rate (ϵ_c) via an order-of-magnitude analysis and suggested a scaling for the square of the second derivative term in Eq. (20). By neglecting higher moments and covariances (see Appendix A) the following approximation can be derived,

$$\frac{\partial}{\partial x_i}\overline{\Big[\rho D_c \frac{\partial c''}{\partial x_i}\Big]} = \beta_0 \beta_1 \frac{\tau}{1 + \tau\widetilde{c}} \overline{S_c} \tag{21}$$

The scaling $\beta_0 \propto Re_t^{1/2}$ [58] was subsequently questioned [59–61] with β_0 here set to unity. Closures for the scalar dissipation rate have advanced beyond algebraic relations [60, 62–64]. A linear algebraic relationship between the scalar dissipation rate and reaction rate is retained in Eq. (21) with β_1 a model constant that follows directly from the relationship between the mean reaction and scalar dissipation rates ($\beta_1 = (2C_m - 1)/2$). Based on Eqs. (18)–(21) extended expressions for the pressure dilatation term in the Reynolds–stress transport equation and the corresponding flamelet pressure scrambling term in the scalar–flux transport equation may accordingly be written as,

$$\overline{p' \frac{\partial u_i''}{\partial x_i}} = C_1(\tau S_L)^2 \overline{S_c}\big(\bar{c} - \frac{1}{2}\big)\Big(1 + \beta_1 \frac{\tau}{1 + \tau\widetilde{c}}\Big) \big\langle \big(\boldsymbol{n} \cdot \boldsymbol{N_i}\big)\big(\boldsymbol{n} \cdot \boldsymbol{N_i}\big) \big\rangle \tag{22}$$

$$\left(\overline{p' \frac{\partial c''}{\partial x_i}}\right)_f = C_2(\tau S_L)\overline{S_c}\big(\bar{c} - \frac{1}{2}\big)\Big(1 + \beta_1 \frac{\tau}{1 + \tau\widetilde{c}}\Big) \big\langle \boldsymbol{n} \cdot \boldsymbol{N_i} \big\rangle \tag{23}$$

where $\boldsymbol{N_i}$ represents the unit vector of flow directions. In particular, $\boldsymbol{N_1}$ stands for the unit

vector of the mean flow direction. The flamelet orientation factor depends on the flowfield and the precise distribution is case–dependent. DNS data has provided statistical averages and the inclusion has been successful in previous studies [65, 66] with $\sigma = \langle \boldsymbol{n} \cdot \boldsymbol{N_1} \rangle = 0.50$ [35, 54] and $\langle (\boldsymbol{n} \cdot \boldsymbol{N_1})(\boldsymbol{n} \cdot \boldsymbol{N_1}) \rangle = 0.50$ [35] used here.

Previous studies [35, 54] suggest that C_1 and C_2 in the dilatation/flamelet scrambling models (i.e. Eqs. (22) and (23)) are lower than unity. Domingo and Bray [35] used 0.50 for both model constants. The introduction of modelling constants C_1 or C_2 cannot guarantee realisability, especially for comparatively low turbulence levels, as the turbulent kinetic energy may approach zero at the flame leading edge as $(\tau S_L) \rightarrow \infty$. However, a "bounded" form for the contribution can readily be formulated,

$$\overline{p' \frac{\partial u_i''}{\partial x_i}} = (\tau S_L)_*^2 \overline{S_c} (\bar{c} - \frac{1}{2}) \Big(1 + \beta_1 \frac{\tau}{1 + \tau \widetilde{c}} \Big) \langle (\boldsymbol{n} \cdot \boldsymbol{N_i})(\boldsymbol{n} \cdot \boldsymbol{N_i}) \rangle \tag{24}$$

$$\left(\overline{p' \frac{\partial c''}{\partial x_i}} \right)_f = (\tau S_L)_* \overline{S_c} (\bar{c} - \frac{1}{2}) \Big(1 + \beta_1 \frac{\tau}{1 + \tau \widetilde{c}} \Big) \langle \boldsymbol{n} \cdot \boldsymbol{N_i} \rangle \tag{25}$$

$$(\tau S_L)_* = \frac{\tau S_L \times (\tau S_L)_{lim}}{\tau S_L + (\tau S_L)_{lim}} \tag{26}$$

The applied value $(\tau S_L)_{lim} = 2.5$ m/s is reasonable for practical hydrocarbon flames where $\tau \sim 6$ and the maximum $S_L \sim 0.45$ m/s and is supported by comparison of model predictions with DNS data as outlined below. It follows that $(\tau S_L)_*$ is strictly bounded with $(\tau S_L)_* \rightarrow 0$ as $\tau S_L \rightarrow 0$, while $(\tau S_L)_* \rightarrow (\tau S_L)_{lim}$ as $\tau S_L \rightarrow \infty$. The form of Eq. (26) also recovers the scaling factor of 0.5 for the flamelet scrambling model as proposed by Domingo and Bray [35] for $(\tau S_L) = (\tau S_L)_{lim}$.

3.2 *Pressure Transport in the Flamelet Regime*

Pressure transport effects are usually neglected in the modelling of turbulent flames. However, such terms can play a role in inhomogeneous turbulence [49]. Furthermore, DNS studies of premixed turbulent flames [15, 17] suggest that pressure transport terms can be of the same order as pressure dilatation terms inside the flame brush. Hence, such transport terms are included via a combination of isothermal and combusting contributions. The isothermal form (*iso*) was developed for turbulent shear flows and contains contributions from bulk convection (rapid) and turbulent diffusion (slow) parts [49],

$$\left(\overline{\frac{\partial p' u_l''}{\partial x_l}} \right)_{iso} = \frac{\partial}{\partial x_l} \Big[C_p f_c \bar{\rho} \frac{\widetilde{u_k'' u_m'' u_m''}}{\widetilde{\epsilon}} \frac{\partial \widetilde{U_p}}{\partial x_k} \widetilde{u_l'' u_p''} + \frac{1}{5} \bar{\rho} \widetilde{u_l'' u_n'' u_n''} \Big] \tag{27}$$

$$\left(\overline{\frac{\partial p' c''}{\partial x_i}} \right)_{iso} = \frac{\partial}{\partial x_i} \Big[C_p f_c \bar{\rho} \frac{\widetilde{u_k'' u_m'' u_m''}}{\widetilde{\epsilon}} \frac{\partial \widetilde{U_p}}{\partial x_k} \widetilde{u_p'' c''} + \frac{1}{5} \bar{\rho} \widetilde{c'' u_n'' u_n''} \Big] \tag{28}$$

where $C_p = 0.40$, $f_c = C_{c1} e^{C_{c2} I}$, $C_{c1} = 0.28$, $C_{c2} = 0.60$, $I = \sqrt{\widetilde{k} / \overline{U_j U_j}}$. Flame-generated pressure transport models remain unavailable [67]. However, a consistent form

for the flamelet regime (f) of combustion can be derived as shown in Appendix B,

$$\left(\overline{\frac{\partial p' u_i''}{\partial x_i}}\right)_f = (\tau S_L)\overline{S_c}\frac{\widetilde{u_i'' c''}}{\widetilde{c}(1-\widetilde{c})}\Big(\widetilde{c} - \frac{(1-\widetilde{c})}{(1+\tau\widetilde{c})}\Big)\langle \boldsymbol{n}\cdot\boldsymbol{N_i}\rangle \tag{29}$$

$$\left(\overline{\frac{\partial p' c''}{\partial x_i}}\right)_f = \overline{S_c}\frac{\widetilde{u_i'' c''}}{\widetilde{c}(1-\widetilde{c})}\Big(\widetilde{c} - \frac{(1-\widetilde{c})}{(1+\tau\widetilde{c})}\Big) \tag{30}$$

The triple–moments in the above equations are obtained via the generalised gradient diffusion hypothesis [68] with C_s assigned the customary value of 0.22.

$$\widetilde{u_i'' u_j'' u_l''} = -C_s\bar{\rho}\frac{\widetilde{k}}{\widetilde{\epsilon}}\widetilde{u_k'' u_l''}\frac{\partial\widetilde{u_i'' u_j''}}{\partial x_k} \tag{31}$$

$$\widetilde{u_i'' u_l'' c''} = -C_s\bar{\rho}\frac{\widetilde{k}}{\widetilde{\epsilon}}\widetilde{u_k'' u_l''}\frac{\partial\widetilde{u_i'' c''}}{\partial x_k} \tag{32}$$

3.3 *Redistribution/Scrambling and Dissipation Correlations*

For the closure of the Reynolds–stress and scalar–flux transport equations, the redistribution/scrambling terms are modelled together with the dissipation terms in the manner of Lindstedt and Váos [31]. The preferential acceleration term, induced by mean pressure gradients, is included through a Isotropisation of Production (IP) type model. The applied Reynolds–stress redistribution and dissipation terms are as follows,

$$\begin{aligned}\phi_{ij}^R - \bar{\rho}\epsilon_{ij} = \bar{\rho}G_{ik}\widetilde{u_k'' u_j''} + \bar{\rho}G_{jk}\widetilde{u_k'' u_i''} + \bar{\rho}\delta_{ij}C_0\widetilde{\epsilon} \\ + C_{A_R}\Big(\Phi_{ij} - \frac{1}{3}\delta_{ij}\Phi_{kk}\Big)\end{aligned} \tag{33}$$

The corresponding closure for the scrambling and dissipation terms follows,

$$\phi_{ic}^S - \bar{\rho}\epsilon_{ic} = \bar{\rho}G_{ik}\widetilde{u_k'' c''} + \bar{\rho}\frac{\widetilde{\epsilon_c}}{\widetilde{c''^2}}\widetilde{u_i'' c''} + C_{A_S}\Phi_{ic} \tag{34}$$

where $C_{A_R} = -3/10, C_{A_S} = -1/3$ [31]. Different values for C_{A_R} have been suggested with Launder [69] recommending -0.6, G_{ij} is a second–rank tensor derived on the basis of the Generalised Langevin Model (GLM). The Haworth and Pope (HP2) model [27] is used along with the Lagrangian (LSSG) version [70] of the SSG model by Speziale et al. [28]. The corresponding expressions and coefficients for the isothermal redistribution/scrambling models are presented in Appendix C.

3.4 *Reaction Rate Closure*

The derived forms of the pressure dilatation/flamelet scrambling terms (Eqs. (24)-(25)) and flamelet pressure transport contribution (Eqs. (29)-(30)) are independent of the form of the reaction rate. Lipatnikov et al. [71] analysed the H, M and L flames (see Table 2) in the same DNS database [17, 18] and showed that, compared to flame surface density expressions, the mean reaction rate is reduced at the leading edge ($\bar{c} < 0.2$) and increased at the trailing edge ($\bar{c} < 0.8$). The former effect, in particular, is important in the current context and a bridged mean reaction rate expression based on the two scale formulation

of Lindstedt and Váos [31] is applied to approximately account for the impact,

$$\widetilde{c} < \widetilde{c}_* : \overline{S_{c1}} = C_{R_1}\rho_u \frac{S_L}{v_K}\frac{\widetilde{\epsilon}}{\widetilde{k}}\widetilde{c}^2\big(1-\widetilde{c}\big) \tag{35}$$

$$\widetilde{c} \geqslant \widetilde{c}_* : \overline{S_{c2}} = C_{R_2}\rho_u \frac{S_L}{v_K}\frac{\widetilde{\epsilon}}{\widetilde{k}}\widetilde{c}\big(1-\widetilde{c}\big) \tag{36}$$

$$\overline{S_{c1}}\;|_{\widetilde{c}_*} = \overline{S_{c2}}\;|_{\widetilde{c}_*} \tag{37}$$

where S_L is the unstrained laminar burning velocity and $v_K = (\nu_0\epsilon)^{1/4}$ the Kolmogorov velocity in the reactants. A value $\widetilde{c}_* = 0.03$ was chosen to approximate the behaviour at the leading edge as shown in Fig. 2. The shapes are different. However, the $c-$space integrals of the bridged mean reaction rate normalised by the expression by Lindstedt and Váos [31] are 0.89, 0.93, 0.96 for the H, M and L flames (see Table 2), in excellent agreement with the corresponding DNS values of 0.88, 0.93, 0.95. The eigenvalue analysis of Catlin and Lindstedt [72] was applied to determine a ratio $C_{R_1}/C_{R_2} = 33.3$ that satisfies Eq. (37). The value $C_{R_2} = 3.8$ ($C_{R_1} = 127$) was obtained by matching the turbulent burning velocities of the DNS studies (see Table 4). For the higher Re_t opposed jet flames the value was adjusted with $C_{R_2} = 3.0$ ($C_{R_1} = 100$). Unclosed reaction–related terms in the scalar-flux transport equation were determined through BML theory [1] with Eq. (39) used only to close Eq. (34).

$$\widetilde{u_i'' S_c} = \frac{\overline{S_c}}{\widetilde{c''^2}}(A_m - \widetilde{c})\widetilde{u_i'' c''} \tag{38}$$

$$\bar{\rho}\frac{\widetilde{\epsilon_c}}{\widetilde{c''^2}} = \frac{\overline{S_c}}{\widetilde{c''^2}}\left(C_m - \frac{1}{2}\right) \tag{39}$$

Chakraborty and Cant [73] introduced A_m as a function of the local turbulent Reynolds number to account for the amount of gradient transport at the leading flame edge of their DNS study and suggest $0.57 \leqslant A_m \leqslant 0.64$ for $10 \leqslant Re_t \leqslant 150$. C_m is also sensitive for small values of $\bar{c}$ due to finite chemistry effects. The implication is that the correlation between chemistry and turbulence is rather sensitive at the leading edge of premixed turbulent flames [74–76]. The current values $A_m = 0.83$ and $C_m = 0.916$ were adopted from Bray and Swaminathan [77].

3.5 *Turbulence Kinetic Energy Dissipation Equation*

The turbulence kinetic energy dissipation equation is required for scale information. The prevalent approach features the standard $k-\epsilon$ model [40],

$$\frac{\partial\bar{\rho}\widetilde{\epsilon}}{\partial t} + \frac{\partial\bar{\rho}\widetilde{u}_l\widetilde{\epsilon}}{\partial x_l} = \frac{\partial}{\partial x_k}\left[C_{s_e}\bar{\rho}\frac{\widetilde{k}}{\widetilde{\epsilon}}\widetilde{u_k'' u_l''}\frac{\partial\widetilde{\epsilon}}{\partial x_l}\right] - C_{\epsilon_1}\bar{\rho}\frac{\widetilde{\epsilon}}{\widetilde{k}}\widetilde{u_k'' u_l''}\frac{\partial\widetilde{u_k}}{\partial x_l} - C_{\epsilon_2}\bar{\rho}\frac{\widetilde{\epsilon}}{\widetilde{k}}\widetilde{\epsilon} - C_{\epsilon_3}\frac{\widetilde{\epsilon}}{\widetilde{k}}\overline{u_l''}\frac{\partial\bar{p}}{\partial x_l} \tag{40}$$

where $C_{S_e} = 0.18, C_{\epsilon_1} = 1.44, C_{\epsilon_2} = 1.92, C_{\epsilon_3} = 1.44$. Here, the Reynolds stresses in the production term are obtained from second–moment transport equations. To be consistent with the Reynolds–stress and scalar–flux transport equations, the present study includes the preferential acceleration terms. An alternative based on the renormalisation

group (RNG) theory [46] has been evaluated in opposed jet flows [47, 48],

$$\frac{\partial\bar{\rho}\widetilde{\epsilon}}{\partial t}+\frac{\partial\bar{\rho}\widetilde{u}_l\widetilde{\epsilon}}{\partial x_l}=\frac{\partial}{\partial x_k}\left[C_{s_e}\bar{\rho}\frac{\widetilde{k}}{\widetilde{\epsilon}}\widetilde{u_k''u_l''}\frac{\partial\widetilde{\epsilon}}{\partial x_l}\right]-\left(C_{\epsilon_1}-\frac{\eta(1-\eta/\eta_0)}{1+\beta\eta^3}\right)\bar{\rho}\frac{\widetilde{\epsilon}}{\widetilde{k}}\widetilde{u_k''u_l''}\frac{\partial\widetilde{u_k}}{\partial x_l}$$
$$-C_{\epsilon_2}\bar{\rho}\frac{\widetilde{\epsilon}}{\widetilde{k}}\widetilde{\epsilon}-C_{\epsilon_3}\frac{\widetilde{\epsilon}}{\widetilde{k}}\overline{u_l''}\frac{\partial\bar{p}}{\partial x_l} \tag{41}$$

with $C_{S_e}=0.18, C_{\epsilon_1}=1.42, C_{\epsilon_2}=1.68, C_{\epsilon_3}=1.44, \eta_0=4.38, \beta=0.012$ and η is related to mean strain rate and the turbulence time scale,

$$\eta=\frac{\widetilde{k}}{\widetilde{\epsilon}}(2a_{ij}a_{ij})^{1/2}\quad a_{ij}=\frac{1}{2}\left(\frac{\partial\widetilde{u}_i}{\partial x_j}+\frac{\partial\widetilde{u}_j}{\partial x_i}\right) \tag{42}$$

4. Application of the Model

The impact of the dilatation/flamelet scrambling models is illustrated by computing premixed (quasi–) one–dimensional planar and two–dimensional axi–symmetric flames. The former enables comparisons with DNS data of statistically “steady" planar flames, while the latter features opposed jet methane-air flames in fractal grid generated turbulence.

4.1 *Case Configuration*

4.1.1 One–Dimensional Planar Flames

Databases [17, 18] used here were generated for fully developed planar premixed flames featuring three different expansion ratios. A single–step irreversible chemical reaction was used to describe the chemistry. Isotropic turbulence was initially assigned to the domain and the mean velocity was carefully controlled to maintain a statistically ‘steady’ flame within the domain. For all cases the initial Re_t is 95.5 with flames crossing the combustion regime boundary between corrugated and wrinkled flamelets. The main initial conditions are summarised in Table 2. The (near) planar nature of the flames suggests a possible approximation using a one–dimensional Favre–averaged Navier–Stokes formulation. The resulting flames propagate normal to themselves in a uniform stream of reactants featuring a constant initial turbulence field extracted from DNS data at the leading edge of the flames [17, 33]. The thermodynamic parameters are consistent with the DNS databases as listed in Table 3. The simulations are transient and the mean velocity of the incoming flow increased gradually until the flame reaches a “steady" state.

4.1.2 Turbulent Opposed Jet Flames

Two–dimensional axi–symmetric computations were performed for experimentally investigated fuel lean premixed turbulent methane–air flames with two equivalence ratios [78]. The bulk velocity at the inlet was 4.0 m/s and, consistent with the experiment, a co-flow with a velocity set to 30% of the bulk flow was used. The Re_t was around 143 based on the integral length scale of 3.47 mm [78]. The flames were estimated to be in the corrugated flamelet regime [79]. The laminar flame properties were obtained from calculations based on detailed chemistry [80] and are listed in Table 5.

4.2 *Numerical Procedure*

All modelling results were obtained from fully transient simulations by using the governing equations integrated in a conservation form as listed in Table 1. The approach features a variable predictor–corrector variant (with splitting error control) of the PISO [81] algorithm for the velocity–pressure coupling with a TVD scheme [82] used to reduce numerical diffusion. A more detailed description of the numerical procedure is available elsewhere [31]. The integral length scale was resolved by 50 computational cells for the one–dimensional cases. The computational domain for the two–dimensional axi–symmetric cases was discretised using a uniform orthogonal 190×39 mesh (radial×axial) with the grid spacing set to 0.4 mm. Grid independence was verified by using a 292×60 mesh.

4.3 *One-Dimensional Flame Calculations*

As shown in Table 2, the DNS databases accessed in the present study feature three expansion ratios of 1.5, 4.0 and 6.53. The flame with the most practical expansion ratio ($\tau = 6.53$) is analysed first to evaluate the effects of the pressure dilatation/flamelet scrambling and pressure transport models on turbulent transport. Having established the formalism, the closure is then applied to flames with diverse expansion ratios. The HP2 model [27] was used as the basis for all three flames.

4.3.1 Pressure Dilatation/Flamelet Scrambling Effects

The impact of pressure dilatation/flamelet scrambling on flame statistics for the H flame is considered first and Table 6 summarises the applied closure variations. The DNS and modelled flames share the same flame brush thickness $L_f \approx 5.0$ mm ($0.005 \leqslant \widetilde{c} \leqslant 0.995$) and statistics are presented within the flame brush ($\widetilde{c}$). Results are shown in Fig. 3 and the second–moment closure (SMC) without “dilatation" terms (Case 1) significantly underestimates the turbulent kinetic energy and the turbulent scalar flux. This implies that “dilatation" effects (Case 2) are significant in the flamelet regime of combustion (e.g. [33, 36, 41]). The closure with the molecular diffusion term (Case 3) further improves agreement in accordance with suggestions regarding the potential importance of such terms [38, 39]. Discrepancies in the turbulent kinetic energy for $\widetilde{c} > 0.7$ are apparent and may stem from highly curved flamelets that envelop “unburned mixture fingers" [83].

The budget of source terms for the turbulent kinetic energy is available for the current DNS database [17] and a comparison of major source terms, as listed in Eq. (43), is made for Case 3. The result is shown in Fig. 4 in physical space normalised by the flame brush thickness $L_f = 5.0$ mm ($0.005 \leqslant \widetilde{c} \leqslant 0.995$).

$$\frac{\partial \widetilde{k}}{\partial t} + \widetilde{u_k}\frac{\partial \widetilde{k}}{\partial x_k} = -\frac{1}{\bar{\rho}}\frac{\partial \overline{\rho u_i'' u_i'' u_k''}}{2\partial x_k} \underbrace{-\frac{\overline{\rho u_i'' u_k''}}{\bar{\rho}}\frac{\partial \widetilde{u}_i}{\partial x_k}}_{\text{Term 1}} \underbrace{-\frac{\overline{u_i''}}{\bar{\rho}}\frac{\partial \bar{p}}{\partial x_i}}_{\text{Term 2}} \underbrace{+\frac{1}{\bar{\rho}}\overline{p'\frac{\partial u_i''}{\partial x_i}}}_{\text{Term 3a}} \underbrace{-\frac{1}{\bar{\rho}}\frac{\partial \overline{p' u_i''}}{\partial x_i}}_{\text{Term 3b}} + \underbrace{\frac{1}{\bar{\rho}}\overline{u_i''\frac{\partial \tau_{ik}}{\partial x_k}}}_{\text{Term 4}} \tag{43}$$

Inspection of Fig. 4(a) reveals that the mean pressure gradient term (Term 2) makes a major positive contribution to the turbulent kinetic energy, while “production” (Term 1) provides a large sink. The agreement with respect to shape and magnitude is satisfactory. As shown in Fig. 4(b), the sum of the pressure dilatation (Term 3a) and the pressure trans-

port (Term 3b) terms is denoted Term 3. It makes a significant positive contribution and the magnitude is well reproduced. The dissipation sink term (Term 4) is well reproduced with respect to the shape though the peak value is somewhat under-predicted. The two components of Term 3: dilatation (Term 3a) and transport (Term 3b), are shown separately in Fig. 4(c). The derived pressure dilatation model (Eq. (24)) provides satisfactory agreement with DNS data. By contrast, the corresponding pressure transport model (Eq. (29)) is significantly smaller than the DNS counterpart and contributes to the shape discrepancy of the overall Term 3 shown in Fig. 4(b). The introduction of a simple scaling factor of 2.5 based on the matching of the peak value provides encouraging quantitative agreement with the DNS data. Model constants were not introduced as pressure transport provides a significant positive contribution at the leading edge of the flame where the reaction rate expression is conjectural. The complete closure denoted by “Extended SMC" is available in Table 1.

4.3.2 Application to Flames with Different Expansion Ratios

The complete closure was further applied to all three cases in the DNS database. Mean velocity and turbulence statistics across the flame brush are compared in Figs. 5-7. Figure 5(a) shows that the predicted mean velocities across the flames are in good agreement with the DNS data for all expansion ratios. Figure 5(b) confirms that the present closure also provides reasonable agreement for the turbulent kinetic energy. The distribution of the turbulent kinetic energy in the normal and cross-stream directions is illustrated in Figs. 6(a) and 6(b). The increase in the cross–stream Reynolds stress ($\widetilde{v''v''}$) only arises from energy transfer via redistribution, pressure dilatation and transport. The flow is clearly very anisotropic and the trends are reproduced. Accordingly, the distribution of the dominant “dilatation" effects using the flamelet orientation angle concept appears effective for planar flames in the flamelet regime of combustion. A comparison of the turbulent scalar flux and DNS data under different expansion ratios is presented in Fig. 7. Counter–gradient transport is observed for all flames with an under-prediction observed at the leading edge of flame L.

4.4 *Opposed Jet Flames*

Data featuring stabilised premixed turbulent twin flames was obtained in the opposed jet configuration by Goh et al. [78]. Variable density effects combine with an imposed mean pressure gradient and the measurements and post–processing by Goh et al. [78] permits the conversion of the (measured) conventional averages to Favre-averaged data using BML based formulations [6] as listed in Appendix D.

Comparisons of Favre-averaged experimental data and simulations are presented in Figs. 8-11, where the nozzle diameter of $D = 30\ \mathrm{mm}$ is used to normalise the positions along the burner centreline. Lower nozzle data are compared with modelled results and error bars are included to show flow asymmetries [78]. Different levels of velocity closures are compared in Fig. 8. It is shown that mean velocities based on second-moment closures are computed with reasonable accuracy; whereas the $k - \epsilon$ model tends to overestimate the contribution within flames. Overall, the high strain rates near the stagnation plane counteract the mean pressure gradient and the flow shares some characteristics of “flames adjacent to walls" where the mean velocity increase is not evident within flames as discussed by Bray et al. [84]. The significant influence of the dilatation model can be readily observed in Fig. 8(b): the turbulent kinetic energy increases notably and the shape of the flame is improved. It is worth mentioning that the alternative model suggested by Lumley [85] increases the maximum of turbulent kinetic energy by 20% as compared to the IP type model and leads to a small over–prediction of the flame thickness. The $k - \epsilon$

model significantly overestimates the turbulent kinetic energy.

The redistribution of the turbulent kinetic energy is illustrated by Fig. 9. It can be seen that further refinement is required near the stagnation plane. The LSSG variant [28, 70] and RNG theory based dissipation equation were introduced in place of the HP2 and standard dissipation models to assess robustness. It can be observed that both alternative closures slightly improve the shape of axial Reynolds stresses ($\widetilde{u''u''}$) but cannot resolve the redistribution issue. Goh et al. [78] recorded the pdf of the rotation of the stagnation plane and the effect, which is not considered in the current simulations, can contribute to the energy transfer. The interactions between the imposed pressure gradient and heat release in opposed jet flames evidently cause additional complications.

Comparisons of the mean reaction progress variable are shown in Fig. 10. The “Extended SMC" predicts an excellent flame shape. Although the $k-\epsilon$ model anchors at a reasonable position, the flame thickness is substantially underestimated. The predicted and measured turbulent scalar flux are compared in physical and scalar space in Fig. 11. Gradient transport can be observed as the imposed pressure gradient outweighs the dilatation effects. However, an increased tendency towards counter-gradient transport is evident for the $\phi = 0.9$ flame. It can be observed that the “Extended SMC" provides improved agreement with the minimum scalar flux for both flames. The computations also agree reasonably well with experimental data for $\phi = 0.8$ and provides satisfactory agreement at the flame trailing edge for $\phi = 0.9$. However, the transition to non–gradient transport is delayed and consistent with an underestimate of the pressure transport term at the leading edge. The $k-\epsilon$ model does not provide a correct flame structure.

5. Conclusions

The present work has illustrated the impact of pressure related terms in the context of premixed turbulent flames with a focus on pressure dilatation and flamelet scrambling terms. The present derivations are consistent with the flamelet regime of combustion wherein the “dilatation" effects are confirmed to be significant. It has also been shown that molecular diffusion and pressure transport make a contribution. Preferential acceleration effects have been introduced in the redistribution and scrambling models in the manner of Lindstedt and Váos [31]. The pressure transport term is modelled via isothermal and variable density parts, with the latter derived for combustion in the flamelet regime in a similar manner to the pressure dilatation/flamelet scrambling models.

A bimodal presumed *pdf* was used in the closure for scalar statistics along with a bridged algebraic expression for the mean reaction rate derived to (partially) mitigate the apparent failure, identified by Lipatnikov et al. [71], of flame surface density based models at the leading edge. Two comprehensive second moment closures [27, 28, 70] were used as the basis for the velocity field calculations and both were found to function well, suggesting practical robustness. By contrast, the commonly used $k-\epsilon$ model was confirmed as an inadequate basis for premixed turbulent flames.

The resulting model was applied to planar flames and opposed jet flames in the flamelet regime of combustion. The accuracy was first analysed by comparisons with DNS data of statistically “steady" planar premixed turbulent flames for which mean pressure gradients accelerate the flow. The influence of dilatation/flamelet scrambling terms was found to be significant with models acting as sources to increase the turbulent kinetic energy and the turbulent scalar flux. The anisotropy of the flowfield was well predicted for different heat release rates. Fuel lean premixed flames in an opposed jet geometry where the mean pressure gradient counteracts the effects of “dilatation" were also computed. Results show that the extended closure improves predictions of both turbulence and scalar statistics. However, a redistribution issue remains close to the stagnation plane and the use of alternative

Reynolds stress (LSSG [28, 70]) and dissipation rate (RNG based [46]) closures do not resolve the issue. It is suggested that the experimentally observed unsteady rotation of the stagnation plane can impact the redistribution of the turbulent kinetic energy. The dynamic competition of mean pressure gradients and dilatation at the leading edge of flames is also enhanced in stagnating flows.

Overall, it has been shown that augmented second–moment based closures can accurately account for pressure dilatation/flamelet scrambling effects. It has also been shown that more comprehensive closures for the reaction rate are desirable, particularly at the leading edge. The latter may include topology based approaches [60–64, 71] or transported *pdf* methods [53, 86–88]. The current work also suggests that pressure – reaction rate terms should be accounted for in LES simulations of premixed turbulent flames as such interactions typically occur on the unresolved scales and can result in significant cross–scale energy transfer [3].

Acknowledgments

The authors wish to gratefully acknowledge communications and data sharing with Vincent Robin, Arnaud Mura and Michel Champion along with discussions with Henry Goh, Fabian Hampp and Evangelos Váos. Lu Tian would like to acknowledge the financial support offered by the Imperial College PhD Scholarship scheme for exceptional students.

References

[1] N. Swaminathan and K.N.C. Bray, *Turbulent Premixed Flames*, Cambridge University Press, Cambridge, 2011.

[2] H. Pitsch, *Large-eddy simulation of turbulent combustion*, Annu. Rev. Fluid Mech. 38 (2006), pp. 453–482.

[3] J. O'Brien, C.A.Z. Towery, P.E. Hamlington, M. Ihme, A.Y. Poludnenko, and J. Urzay, *The cross-scale physical-space transfer of kinetic energy in turbulent premixed flames*, Proc. Combust. Inst. 36 (2016), pp. 1967–1975.

[4] C.Y. Lee, L.K.B. Li, M.P. Juniper, and R.S. Cant, *Nonlinear hydrodynamic and thermoacoustic oscillations of a bluff-body stabilised turbulent premixed flame*, Combust. Theor. and Model. 20 (2016), pp. 131–153.

[5] P.A. Libby, *Theory of normal premixed turbulent flames revisited*, Prog. Energ. Combust. 11 (1985), pp. 83–96.

[6] K.N.C. Bray, P.A. Libby, and J.B. Moss, *Unified modeling approach for premixed turbulent combustion-part i: general formulation*, Combust. Flame 61 (1985), pp. 87–102.

[7] K.N.C. Bray, *Studies of the turbulent burning velocity*, P. R. Soc. Lon. Ser.-A. 431 (1990), pp. 315–335.

[8] N. Peters, *Turbulent Combustion*, Cambridge University Press, 2000.

[9] S. Nambully, P. Domingo, V. Moureau, and L. Vervisch, *A filtered-laminar-flame PDF sub-grid scale closure for LES of premixed turbulent flames. part i: Formalism and application to a bluff-body burner with differential diffusion*, Combust. Flame 161 (2014), pp. 1756–1774.

[10] D. Butz, Y. Gao, A.M. Kempf, and N. Chakraborty, *Large eddy simulations of a turbulent premixed swirl flame using an algebraic scalar dissipation rate closure*, Combust. Flame 162 (2015), pp. 3180–3196.

[11] V. Sabelnikov, A. Lipatnikov, N. Chakraborty, S. Nishiki, and T. Hasegawa, *A transport equation for reaction rate in turbulent flows*, Phys. Fluids 28 (2016), p. 081701.

[12] M. Heitor, A. Taylor, and J. Whitelaw, *The interaction of turbulence and pressure gradients in a baffle-stabilized premixed flame*, J. Fluid Mech. 181 (1987), pp. 387–413.

[13] K.H.H. Goh, P. Geipel, and R.P. Lindstedt, *Turbulent transport in premixed flames approaching extinction*, Proc. Combust. Inst. 35 (2014), pp. 1469–1476.

[14] B. Coriton, J.H. Frank, and A. Gomez, *Effects of strain rate, turbulence, reactant stoichiometry and heat losses on the interaction of turbulent premixed flames with stoichiometric counterflowing combustion products*, Combust. Flame 160 (2013), pp. 2442–2456.

[15] C.J. Rutland and R.S. Cant, *Turbulent transport in premixed flames*, in *Proceedings of the Summer Program*, Stanford, CA, 1994, pp. 75–94.

[16] D. Veynante and T. Poinsot, *Effects of pressure gradients on turbulent premixed flames*, J. Fluid Mech. 353 (1997), pp. 83–114.

[17] S. Nishiki, T. Hasegawa, R. Borghi, and R. Himeno, *Modeling of flame-generated turbulence based on direct numerical simulation databases*, Proc. Combust. Inst. 29 (2002), pp. 2017–2022.

[18] S. Nishiki, T. Hasegawa, R. Borghi, and R. Himeno, *Modelling of turbulent scalar flux in turbulent premixed flames based on DNS databases*, Combust. Theor. Model. 10 (2006), pp. 39–55.

[19] L. Cifuentes, C. Dopazo, J. Martín, P. Domingo, and L. Vervisch, *Local volumetric dilatation rate and scalar geometries in a premixed methane–air turbulent jet flame*, Proc. Combust. Inst. 35 (2015), pp. 1295–1303.

[20] K.N.C. Bray, P.A. Libby, G. Masuya, and J. Moss, *Turbulence production in premixed turbulent flames*, Combust. Sci. Technol. 25 (1981), pp. 127–140.

[21] S. Zhang and C.J. Rutland, *Premixed flame effects on turbulence and pressure-related terms*, Combust. Flame 102 (1995), pp. 447–461.

[22] T. Treurniet, F. Nieuwstadt, and B. Boersma, *Direct numerical simulation of homogeneous turbulence in combination with premixed combustion at low Mach number modelled by the G-equation*, J. Fluid Mech. 565 (2006), pp. 25–62.

[23] A. Trouvé, D. Veynante, K.N.C. Bray, and T. Mantel, *The coupling between flame surface dynamics and species mass conservation in premixed turbulent combustion*, in *Proceedings of the Summer Program*, Stanford, CA, 1994, pp. 95–124.

[24] D. Veynante, A. Trouvé, K.N.C. Bray, and T. Mantel, *Gradient and counter-gradient scalar transport in turbulent premixed flames*, J. Fluid Mech. 332 (1997), pp. 263–293.

[25] S. Nishiki, *DNS and modeling of turbulent premixed combustion*, Ph.D. diss., Nagoya Institute of Technology (Japan), 2003.

[26] D. Haworth and S. Pope, *A generalized Langevin model for turbulent flows*, Phys. Fluids 29 (1986), pp. 387–405.

[27] D. Haworth and S. Pope, *A PDF modeling study of self-similar turbulent free shear flows*, Phys. Fluids 30 (1987), pp. 1026–1044.

[28] C.G. Speziale, S. Sarkar, and T.B. Gatski, *Modelling the pressure–strain correlation of turbulence: an invariant dynamical systems approach*, J. Fluid Mech. 227 (1991), pp. 245–272.

[29] P. Bailly, M. Champion, and D. Garréton, *Counter-gradient diffusion in a confined turbulent premixed flame*, Phys. Fluids 9 (1997), pp. 766–775.

[30] D. Karmed, M. Champion, and P. Bruel, *Two-dimensional numerical modeling of a turbulent premixed flame stabilized in a stagnation flow*, Combust. Flame 119 (1999), pp. 335–345.

[31] R.P. Lindstedt and E.M. Váos, *Modeling of premixed turbulent flames with second moment methods*, Combust. Flame 116 (1999), pp. 461–485.

[32] M. Gibson and B. Launder, *On the calculation of horizontal, turbulent, free shear flows under gravitational influence*, J. Heat Transf. 98 (1976), pp. 81–87.

[33] V. Robin, A. Mura, and M. Champion, *Direct and indirect thermal expansion effects in turbulent premixed flames*, J. Fluid Mech. 689 (2011), pp. 149–182.

[34] V. Kuznetsov, *Estimate of the correlation between pressure pulsations and the divergence of the velocity in subsonic flows of variable density*, Fluid Dyn. 14 (1979), pp. 328–334.

[35] P. Domingo and K.N.C. Bray, *Laminar flamelet expressions for pressure fluctuation terms in second moment models of premixed turbulent combustion*, Combust. Flame 121 (2000), pp. 555–574.

[36] T. Hůlek and R.P. Lindstedt, *Modelling of unclosed nonlinear terms in a PDF closure for turbulent flames*, Math. Comput. Model. 24 (1996), pp. 137–147.

[37] W.P. Jones, *Turbulence modelling and numerical solution methods for variable density and combusting flows*, in *Turbulent Reacting Flows*, P.A. Libby and F.A. Williams, eds., book section 6, Academic Press, Cambridge, MA (1994), pp. 309–347.

[38] D.H. Rowinski and S.B. Pope, *Computational study of lean premixed turbulent flames using RANS–PDF and LES–PDF methods*, Combust. Theor. and Model. 17 (2013), pp. 610–656.

[39] R.R. Tirunagari and S.B. Pope, *An investigation of turbulent premixed counterflow flames using large-eddy simulations and probability density function methods*, Combust. Flame 166 (2016), pp. 229–242.

[40] W. Jones and B. Launder, *The prediction of laminarization with a two-equation model of turbulence*, Int. J. Heat Mass Tran. 15 (1972), pp. 301–314.

[41] A. Mura and M. Champion, *Relevance of the Bray number in the small-scale modeling of turbulent premixed flames*, Combust. Flame 156 (2009), pp. 729–733.

[42] R. Borghi and D. Escudie, *Assessment of a theoretical model of turbulent combustion by comparison with a simple experiment*, Combust. Flame 56 (1984), pp. 149–164.

[43] R.S. Cant and K.N.C. Bray, *A theoretical model of premixed turbulent combustion in closed vessels*, Combust. Flame 76 (1989), pp. 243–263.

[44] D. Bradley, P. Gaskell, and X. Gu, *Application of a Reynolds stress, stretched flamelet, mathemati-*

cal model to computations of turbulent burning velocities and comparison with experiments, Combust. Flame 96 (1994), pp. 221–248.

[45] R.P. Lindstedt and E.M. Váos, *Second moment modeling of premixed turbulent flames stabilized in impinging jet geometries*, Proc. Combust. Inst. 27 (1998), pp. 957–962.

[46] V. Yakhot, S. Orszag, S. Thangam, T. Gatski, and C. Speziale, *Development of turbulence models for shear flows by a double expansion technique*, Phys. Fluids 4 (1992), pp. 1510–1520.

[47] R.P. Lindstedt, D.S. Luff, and J.H. Whitelaw, *Velocity and strain-rate characteristics of opposed isothermal flows*, Flow Turbul. Combust. 74 (2005), pp. 169–194.

[48] R.P. Lindstedt, D.S. Luff, and J.H. Whitelaw, *Velocity fields of fuel lean premixed turbulent opposed jet flames*, Proc. Combust. Inst. 31 (2007), pp. 1459–1466.

[49] S.K. Kim and M.K. Chung, *Spatial transport of Reynolds stresses by pressure fluctuations*, Phys. Fluids 6 (1994), pp. 3507–3509.

[50] R. Borghi, *On the structure and morphology of turbulent premixed flames*, in *Recent Advances in the Aerospace Sciences*, Springer, New York (1985), pp. 117–138.

[51] J. Jeans and J.H. Jeans, *An Introduction to the Kinetic Theory of Gases*, Cambridge University Press, Cambridge, 1982.

[52] H. Kolla and N. Swaminathan, *Strained flamelets for turbulent premixed flames ii: Laboratory flame results*, Combust. Flame 157 (2010), pp. 1274–1289.

[53] T. Hůlek and R.P. Lindstedt, *Computations of steady-state and transient premixed turbulent flames using PDF methods*, Combust. Flame 104 (1996), pp. 481–504.

[54] T. Poinsot and D. Veynante, *Flame surface density models*, in *Theoretical and Numerical Combustion*, book section 5, RT Edwards, Inc., Philadelphia, PA (2005), pp. 224–232.

[55] Y. Zhang, K.N.C. Bray, and B. Rogg, *The modelling and measurement of local flame surface orientation in turbulent premixed flames*, Combust. Sci. Technol. 137 (1998), pp. 347–358.

[56] B. Renou, A. Mura, E. Samson, and A. Boukhalfa, *Characterization of the local flame structure and the flame surface density for freely propagating premixed flames at various Lewis numbers*, Combust. Sci. Technol. 174 (2002), pp. 143–179.

[57] N. Swaminathan, R. Bilger, and G. Ruetsch, *Interdependence of the instantaneous flame front structure and the overall scalar flux in turbulent premixed flames*, Combust. Sci. Technol. 128 (1997), pp. 73–97.

[58] T. Mantel and R. Borghi, *A new model of premixed wrinkled flame propagation based on a scalar dissipation equation*, Combust. Flame 96 (1994), pp. 443–457.

[59] E.M. Váos, *Modelling of the dissipation rate of scalar fluctuations in turbulent flows*, Master diss., Imperial College London, 1993.

[60] N. Chakraborty, M. Champion, A. Mura, and N. Swaminathan, *Scalar dissipation rate approach*, in *Turbulent Premixed Flames*, N. Swaminathan and K.N.C. Bray, eds., Cambridge University Press, Cambridge (2011), pp. 74–102.

[61] A. Mura and R. Borghi, *Towards an extended scalar dissipation equation for turbulent premixed combustion*, Combust. Flame 133 (2003), pp. 193–196.

[62] N. Chakraborty, J. Rogerson, and N. Swaminathan, *A priori assessment of closures for scalar dissipation rate transport in turbulent premixed flames using direct numerical simulation*, Phys. Fluids 20 (2008), p. 045106.

[63] H. Kolla, J.W. Rogerson, N. Chakraborty, and N. Swaminathan, *Scalar dissipation rate modeling and its validation*, Combust. Sci. Technol. 181 (2009), pp. 518–535.

[64] Y. Gao, N. Chakraborty, and N. Swaminathan, *Scalar dissipation rate transport in the context of large eddy simulations for turbulent premixed flames with non-unity Lewis number*, Flow Turbul. Combust. 93 (2014), pp. 461–486.

[65] V. Robin, M. Champion, and A. Mura, *A second-order model for turbulent reactive flows with variable equivalence ratio*, Combust. Sci. and Technol 180 (2008), pp. 1709–1734.

[66] V. Robin, A. Mura, M. Champion, and T. Hasegawa, *A new analysis of the modeling of pressure fluctuations effects in premixed turbulent flames and its validation based on DNS data*, Combust. Sci. and Technol. 180 (2008), pp. 997–1010.

[67] A. Lipatnikov and J. Chomiak, *Effects of premixed flames on turbulence and turbulent scalar transport*, Prog. Energ. Combust. 36 (2010), pp. 1–102.

[68] B.J. Daly and F.H. Harlow, *Transport equations in turbulence*, Phys. Fluids 13 (1970), pp. 2634–2649.

[69] B.E. Launder, *Second-moment closure: present and future?*, Int. J. Heat Fluid Fl. 10 (1989), pp. 282–300.

[70] S.B. Pope, *On the relationship between stochastic Lagrangian models of turbulence and second–moment closures*, Phys. Fluids 6 (1994), pp. 973–985.

[71] A.N. Lipatnikov, V.A. Sabelnikov, S. Nishiki, and T. Hasegawa, *Flamelet perturbations and flame surface density transport in weakly turbulent premixed combustion*, Combust. Theor. and Model. 21 (2017), pp. 205–227.

[72] C. Catlin and R. Lindstedt, *Premixed turbulent burning velocities derived from mixing controlled reaction models with cold front quenching*, Combust. Flame 85 (1991), pp. 427–439.

[73] N. Chakraborty and R.S. Cant, *Effects of turbulent Reynolds number on turbulent scalar flux modeling in premixed flames using Reynolds-averaged Navier-Stokes simulations*, Numer. Heat Tr. A-Appl. 67 (2015), pp. 1187–1207.

[74] A.N. Lipatnikov, S. Nishiki, and T. Hasegawa, *DNS assessment of relation between mean reaction and scalar dissipation rates in the flamelet regime of premixed turbulent combustion*, Combust. Theor. and Model. 19 (2015), pp. 309–328.

[75] V.A. Sabelnikov and A.N. Lipatnikov, *Transition from pulled to pushed premixed turbulent flames due to countergradient transport*, Combust. Theor. and Model. 17 (2013), pp. 1154–1175.

[76] K.Q.N. Kha, V. Robin, A. Mura, and M. Champion, *Implications of laminar flame finite thickness on the structure of turbulent premixed flames*, J. Fluid Mech. 787 (2016), pp. 116–147.

[77] K.N.C. Bray and N. Swaminathan, *Laminar flamelets and the Bray, Moss, and Libby model*, in *Turbulent Premixed Flames*, N. Swaminathan and K.N.C. Bray, eds., Cambridge University Press, Cambridge (2011), pp. 41–60.

[78] K.H.H. Goh, P. Geipel, and R.P. Lindstedt, *Lean premixed opposed jet flames in fractal grid generated multiscale turbulence*, Combust. Flame 161 (2014), pp. 2419–2434.

[79] K.H.H. Goh, *Investigation of conditional statistics in premixed combustion and the transition to flameless oxidation in turbulent opposed jets*, Ph.D. diss., Imperial College London, 2013.

[80] R.K. Robinson and R.P. Lindstedt, *On the chemical kinetics of cyclopentadiene oxidation*, Combust. Flame 158 (2011), pp. 666–686.

[81] R.I. Issa, *Solution of the implicitly discretised fluid flow equations by operator-splitting*, J. Comput. Phys. 62 (1986), pp. 40–65.

[82] P.K. Sweby, *High resolution schemes using flux limiters for hyperbolic conservation laws*, SIAM J. on Numerical Analysis 21 (1984), pp. 995–1011.

[83] A.N. Lipatnikov, J. Chomiak, V.A. Sabelnikov, S. Nishiki, and T. Hasegawa, *Unburned mixture fingers in premixed turbulent flames*, Proc. Combust. Inst. 35 (2015), pp. 1401–1408.

[84] K.N.C. Bray, M. Champion, and P.A. Libby, *Premixed flames in stagnating turbulence part ii. the mean velocities and pressure and the Damköhler number*, Combust. Flame 112 (1998), pp. 635–653.

[85] J.L. Lumley, *Computational modeling of turbulent flows*, Adv. Appl. Mech. 18 (1979), pp. 123–176.

[86] M.S. Anand and S.B. Pope, *Calculations of premixed turbulent flames by PDF methods*, Combust. Flame 67 (1987), pp. 127–142.

[87] R.P. Lindstedt and E.M. Váos, *Transported PDF modeling of high-Reynolds-number premixed turbulent flames*, Combust. Flame 145 (2006), pp. 495–511.

[88] R.P. Lindstedt, V.D. Milosavljevic, and M. Persson, *Turbulent burning velocity predictions using transported PDF methods*, Proc. Combust. Inst. 33 (2011), pp. 1277–1284.

[89] R. Bilger, *Conditional moment closure for turbulent reacting flow*, Phys. Fluids 5 (1993), pp. 436–444.

[90] A.Y. Klimenko and R.W. Bilger, *Conditional moment closure for turbulent combustion*, Prog. energ. combust. 25 (1999), pp. 595–687.

Appendix A. Derivation of pressure dilatation/flamelet scrambling models

In the flamelet regime of combustion, the pressure dilatation term can be expressed as [21],

$$\overline{p'\frac{\partial u_i''}{\partial x_i}} = \frac{1}{V}\int_V p'\frac{\partial u_i''}{\partial x_i}\mathrm{d}V = \frac{S}{V}\Big\langle \int_\xi p'\frac{\partial u_i''}{\partial x_i}\mathrm{d}\xi\Big\rangle_s \tag{A1}$$

The coordinate is shown in Fig. 1. $\boldsymbol{n}$ is the unit vector of axis ξ, pointing from reactants to products; while $\boldsymbol{N_i}$ stands for the unit vector of axis x_i. It is noted that "dilatation" effects within flamelets accelerate the velocity field u_n normal to the flame front (e.g. [33]) with u_i, the projection of u_n, on axis x_i. To evaluate Eq. (A1),

$$\frac{\partial u_i''}{\partial x_i} \simeq \frac{\mathrm{d}u_i}{\mathrm{d}x_i} = \frac{\mathrm{d}u_i}{\mathrm{d}\xi}\frac{\mathrm{d}\xi}{\mathrm{d}x_i} = \frac{\mathrm{d}u_n}{\mathrm{d}\xi}\frac{\mathrm{d}u_i}{\mathrm{d}u_n}\frac{\mathrm{d}\xi}{\mathrm{d}x_i} \tag{A2}$$

$$\frac{\mathrm{d}u_i}{\mathrm{d}u_n} = \frac{\mathrm{d}\xi}{\mathrm{d}x_i} = \boldsymbol{n}\cdot\boldsymbol{N_i} \tag{A3}$$

and substitutions of Eqs. (A2) and (A3) into Eq. (A1) give,

$$\overline{p'\frac{\partial u_i''}{\partial x_i}} = \Sigma\Big\langle \int_{u_n} p'\mathrm{d}u_n\Big\rangle_s\Big\langle\big(\boldsymbol{n}\cdot\boldsymbol{N_i}\big)\big(\boldsymbol{n}\cdot\boldsymbol{N_i}\big)\Big\rangle \tag{A4}$$

The integral in Eq. (A4) can be obtained using the one-dimensional momentum equation [21, 53],

$$\overline{p'\frac{\partial u_i''}{\partial x_i}} = \overline{S_c}(\tau S_L)^2\big(\frac{<p_u-\overline{p}>_s}{\triangle p} - \frac{1}{2}\big)\Big\langle\big(\boldsymbol{n}\cdot\boldsymbol{N_i}\big)\big(\boldsymbol{n}\cdot\boldsymbol{N_i}\big)\Big\rangle \tag{A5}$$

$$\triangle p = \rho_u S_L^2\tau$$

The current work adopts the expression in Eq. (A6) [36]

$$<p_u-\overline{p}>_s = \bar{c}\triangle p \tag{A6}$$

and substitution of Eq. (A6) into Eq. (A5) gives,

$$\overline{p'\frac{\partial u_i''}{\partial x_i}} = \overline{S_c}(\tau S_L)^2\big(\bar{c} - \frac{1}{2}\big)\Big\langle\big(\boldsymbol{n}\cdot\boldsymbol{N_i}\big)\big(\boldsymbol{n}\cdot\boldsymbol{N_i}\big)\Big\rangle \tag{A7}$$

The corresponding pressure flamelet scrambling term follows as,

$$\left(\overline{p'\frac{\partial c''}{\partial x_i}}\right)_f = \Sigma\Big\langle\int_\xi p'\frac{\partial c''}{\partial x_i}\mathrm{d}\xi\Big\rangle_s = \Sigma\Big\langle\int_\xi p'\frac{\mathrm{d}c}{\mathrm{d}\xi}\mathrm{d}\xi\Big\rangle_s\big\langle\boldsymbol{n}\cdot\boldsymbol{N_i}\big\rangle \tag{A8}$$

where $(\ )_f$ indicates the flamelet contribution. The continuity equation for a steady state laminar flame and gives,

$$u_n = (1+\tau c)S_L \tag{A9}$$

Differentiation of Eq. (A9) (e.g. $\mathrm{d}c = \frac{1}{\tau S_L}\mathrm{d}u_n$) links Eq. (A8) with Eq. (A7),

$$\left(\overline{p'\frac{\partial c''}{\partial x_i}}\right)_f = \overline{S_c}(\tau S_L)\big(\bar{c}-\frac{1}{2}\big)\big\langle \boldsymbol{n}\cdot\boldsymbol{N_i}\big\rangle \tag{A10}$$

Use of the instantaneous continuity and scalar equations and the linear relationship between the reaction progress variable (c) and specific volume ($1/\rho$) suggests a more comprehensive expression of the pressure dilatation term

$$\overline{p'\frac{\partial u_i''}{\partial x_i}} = \overline{p'\frac{\partial}{\partial x_i}\Big[\rho D_c\frac{\partial c''}{\partial x_i}\Big]\frac{\partial \rho^{-1}}{\partial c}} + \overline{p'S_c\frac{\partial \rho^{-1}}{\partial c}} \tag{A11}$$

where D_c represents the molecular diffusion coefficient. Equation (A7) is, in fact, a model of the second term in Eq. (A11) and according to the mean value theorem, there exists a flame surface average $\big\langle p'\big\rangle_s$ satisfying the relation.

$$\begin{aligned}\overline{p'S_c\frac{\partial \rho^{-1}}{\partial c}} &= (\tau S_L)^2\overline{S_c}\big(\bar{c}-\frac{1}{2}\big)\big\langle\big(\boldsymbol{n}\cdot\boldsymbol{N_i}\big)\big(\boldsymbol{n}\cdot\boldsymbol{N_i}\big)\big\rangle \\ &= \frac{\tau}{\rho_u}\overline{S_c}\big\langle p'\big\rangle_s\end{aligned} \tag{A12}$$

Mantel and Borghi [58] developed a modelled transport equation for the scalar dissipation rate and suggested the following proportionality,

$$D_c^2\overline{(\frac{\partial}{\partial x_i}\Big[\frac{\partial c'}{\partial x_k}\Big])^2} \sim \beta_0\frac{\overline{\epsilon_c}^2}{\overline{c'^2}} \tag{A13}$$

where β_0 is a model constant and D_c represents the molecular diffusivity. The scaling is not directly applicable in the current context. However, it can provide guidance if assumptions similar to first-order Conditional Moment Closure (CMC) or flamelet models [8, 89, 90] are introduced. Hence, by neglecting fluctuations in (i) the scalar dissipation rate, (ii) the variance and (iii) the second derivative of c', the following results,[1]

$$\overline{\frac{1}{c'^2}} \approx \frac{1}{\overline{c'^2}} \tag{A14}$$

$$\overline{\epsilon_c}^2 \approx \overline{(\epsilon_c)^2} \tag{A15}$$

$$\overline{(\frac{\partial}{\partial x_i}\Big[\frac{\partial c'}{\partial x_k}\Big])^2} \approx \left(\frac{\partial}{\partial x_i}\overline{\Big[\frac{\partial c'}{\partial x_k}\Big]}\right)^2 \tag{A16}$$

Equations (A14)-(A16) combined with the assumption that the covariance of ϵ_c^2 and $1/c'^2$ is sufficiently lower than the product of their means gives,

$$\left(D_c\frac{\partial}{\partial x_i}\overline{\Big[\frac{\partial c'}{\partial x_k}\Big]}\right)^2 \sim \left(\overline{\Big(\frac{\epsilon_c}{c'}\Big)}\right)^2 \tag{A17}$$

[1]The use of a Taylor series expansion for a property $a = \overline{a} + a'$ and with $\frac{a'}{\overline{a}} \to 0$ gives $\overline{\frac{1}{a}} = \overline{\frac{1}{\overline{a}}\frac{1}{(1+\frac{a'}{\overline{a}})}} = \overline{\frac{1}{\overline{a}}(1-\frac{a'}{\overline{a}}+2(\frac{a'}{\overline{a}})^2-...)} \approx \frac{1}{\overline{a}}$.

The result may be rewritten using Favre averages with the assumption of constant D_c,

$$\left(D_c\frac{\partial}{\partial x_i}\overline{\Big[\rho\frac{\partial c''}{\partial x_k}\Big]}\right)^2 \approx \left(\frac{\partial}{\partial x_i}\overline{\Big[\rho D_c\frac{\partial c''}{\partial x_k}\Big]}\right)^2 \sim \left(\overline{\Big(\frac{\rho\epsilon_c}{c''}\Big)}\right)^2 \tag{A18}$$

The instantaneous scalar dissipation rate is proportional to the instantaneous chemical reaction rate [60]. Also, with the assumed "separation" of flame and turbulence and the BML theory based Eq. (7), we have,

$$\overline{\Big(\frac{\rho\epsilon_c}{c''}\Big)} = \beta_1\overline{\Big(\frac{S_c}{c''}\Big)} = \beta_1\Sigma\big\langle\int\frac{S_c}{c''}\mathrm{d}\xi\big\rangle_s = \beta_1\frac{\tau}{1+\tau\widetilde{c}}\overline{S_c} \tag{A19}$$

where $\beta_1 = 0.42$, which follows the coefficient between mean reaction rate and mean scalar dissipation rate ($\beta_1 = (2C_m - 1)/2$). The above approximation is intended to provide a leading order estimate. The diagonal terms $\frac{\partial}{\partial x_i}\overline{\Big[\rho D_c\frac{\partial c''}{\partial x_i}\Big]}$ were studied by Swaminathan et al. [57] and found to provide significant positive contributions especially at the leading flame edge – consistent with the derived expression. Use of the linear thermochemical relationship between the reaction progress variable (c) and the gas specific volume ($1/\rho$), the mean value theorem and Eqs. (A18)–(A19) gives,

$$\begin{aligned}\overline{p'\frac{\partial}{\partial x_i}\Big[\rho D_c\frac{\partial c''}{\partial x_i}\Big]\frac{\partial\rho^{-1}}{\partial c}} &= \big\langle p'\big\rangle_s\frac{\tau}{\rho_u}\frac{\partial}{\partial x_i}\overline{\Big[\rho D_c\frac{\partial c''}{\partial x_i}\Big]}\\ &= \beta_1\frac{\tau}{\rho_u}\big\langle p'\big\rangle_s\frac{\tau}{1+\tau\widetilde{c}}\overline{S_c}\end{aligned} \tag{A20}$$

Finally, Eq. (A20) may be rewritten via Eq. (A12),

$$\overline{p'\frac{\partial}{\partial x_i}\Big[\rho D_c\frac{\partial c''}{\partial x_i}\Big]\frac{\partial\rho^{-1}}{\partial c}} = \beta_1(\tau S_L)^2\overline{S_c}\big(\bar{c}-\frac{1}{2}\big)\Big(\frac{\tau}{1+\tau\widetilde{c}}\Big)\big\langle\big(\boldsymbol{n}\cdot\boldsymbol{N_i}\big)\big(\boldsymbol{n}\cdot\boldsymbol{N_i}\big)\big\rangle \tag{A21}$$

With the introduction of limiter $(\tau S_L)_*$ to guarantee realisability, the pressure dilatation/flamelet scrambling models can accordingly be written as,

$$\overline{p'\frac{\partial u_i''}{\partial x_i}} = (\tau S_L)_*{}^2\overline{S_c}\big(\bar{c}-\frac{1}{2}\big)\Big(1+\beta_1\frac{\tau}{1+\tau\widetilde{c}}\Big)\big\langle\big(\boldsymbol{n}\cdot\boldsymbol{N_i}\big)\big(\boldsymbol{n}\cdot\boldsymbol{N_i}\big)\big\rangle \tag{A22}$$

$$\left(\overline{p'\frac{\partial c''}{\partial x_i}}\right)_f = (\tau S_L)_*\overline{S_c}\big(\bar{c}-\frac{1}{2}\big)\Big(1+\beta_1\frac{\tau}{1+\tau\widetilde{c}}\Big)\big\langle\boldsymbol{n}\cdot\boldsymbol{N_i}\big\rangle \tag{A23}$$

$$(\tau S_L)_* = \frac{\tau S_L + (\tau S_L)_{lim}}{\tau S_L(\tau S_L)_{lim}} \tag{A24}$$

where $(\tau S_L)_{lim} = 2.5$ m/s.

Appendix B. Derivation of flame-generated pressure transport models

Consistent with Appendix A, the volume average of the pressure transport term can be written as a flame surface average,

$$\left(\overline{\frac{\partial p' u_i''}{\partial x_i}}\right)_f = \frac{1}{V}\int_V \frac{\partial p' u_i''}{\partial x_i}\mathrm{d}V = \frac{S}{V}\Big\langle \int_\xi \frac{\partial p' u_i''}{\partial x_i}\mathrm{d}\xi \Big\rangle_s \tag{B1}$$

where $<>_s$ represents a flame surface average. Following the coordinates shown in Fig. 1, Eq. (B1) can be rewritten as,

$$\left(\overline{\frac{\partial p' u_i''}{\partial x_i}}\right)_f = \frac{S}{V}\Big\langle \int_\xi \frac{\mathrm{d}p' u_i''}{\mathrm{d}x_i}\mathrm{d}x_i \Big\rangle_s \big\langle \boldsymbol{n}\cdot\boldsymbol{N_i}\big\rangle \tag{B2}$$

$$= \frac{S}{V}\big\langle p' u_i''|_u^b \big\rangle_s \big\langle \boldsymbol{n}\cdot\boldsymbol{N_i}\big\rangle \tag{B3}$$

$$= \frac{S}{V}\big\langle \boldsymbol{n}\cdot\boldsymbol{N_i}\big\rangle \big[(p_b-\bar{p})(u_{ib}-\widetilde{u_i}) - (p_u-\bar{p})(u_{iu}-\widetilde{u_i})\big] \tag{B4}$$

where the subscripts *b* and *u* stand for burnt products and unburnt reactants.

$$\widetilde{u_i'' c''} = \widetilde{c}(1-\widetilde{c})(\overline{u_i}_b - \overline{u_i}_u) \tag{B5}$$

$$\overline{u_i}_b = \widetilde{u_i} - \frac{\widetilde{u_i'' c''}}{1-\widetilde{c}} \tag{B6}$$

$$\overline{u_i}_u = \widetilde{u_i} + \frac{\widetilde{u_i'' c''}}{\widetilde{c}} \tag{B7}$$

It is assumed that the velocities in the products and reactants can be represented by the conditional velocities ($u_{ib} \approx \overline{u_i}_b$ and $u_{iu} \approx \overline{u_i}_u$). The BML formalism [1, 20] provides Eqs. (B5)-(B7) combined with the applied pressure differences,

$$p_b - \bar{p} = (1-\bar{c})\triangle p = (1-\bar{c})\rho_u \tau S_L^2 \tag{B8}$$

$$p_u - \bar{p} = \bar{c}\triangle p = \bar{c}\rho_u \tau S_L^2 \tag{B9}$$

Substitutions of Eqs. (B6)-(B9) into Eq. (B2), the conversion from the conventional to Favre average of reaction progress variable based on BML theory [6] and the expression for the mean reaction rate based on flame surface density lead to,

$$\left(\overline{\frac{\partial p' u_i''}{\partial x_i}}\right)_f = \big\langle \boldsymbol{n}\cdot\boldsymbol{N_i}\big\rangle (\tau S_L)\overline{S_c}\frac{\widetilde{u_i'' c''}}{\widetilde{c}(1-\widetilde{c})}\Big(\widetilde{c} - \frac{(1-\widetilde{c})}{(1+\tau\widetilde{c})}\Big) \tag{B10}$$

Similarly, we can obtain the corresponding pressure transport model for the scalar flux via Eqs. (A9) and (A3),

$$\left(\overline{\frac{\partial p' c''}{\partial x_i}}\right)_f = \frac{\widetilde{u_i'' c''}}{\widetilde{c}(1-\widetilde{c})}\overline{S_c}\Big(\widetilde{c} - \frac{(1-\widetilde{c})}{(1+\tau\widetilde{c})}\Big) \tag{B11}$$

Appendix C. G_{ij} Tensor

$$\phi_{ij}^{CD} = \bar{\rho}\left(\frac{\widetilde{\epsilon}}{\widetilde{k}}C_{ij}[\mathbf{b}] + B_{ijkl}[\mathbf{b}]\frac{\partial\widetilde{u_k}}{\partial x_l}\right)\widetilde{k} \tag{C1}$$

$$= \bar{\rho}G_{ik}\widetilde{u_k''u_j''} + \bar{\rho}G_{jk}\widetilde{u_k''u_i''} + \bar{\rho}\left(C_0 + \frac{2}{3}\right)\delta_{ij}\widetilde{\epsilon} \tag{C2}$$

$$\phi_{ic}^{CD} = \bar{\rho}\left(\frac{\widetilde{\epsilon}}{\widetilde{k}}C_{ij}^{f}[\mathbf{b}] + B_{ijkl}^{f}[\mathbf{b}]\frac{\partial\widetilde{u_k}}{\partial x_l}\right)\widetilde{u_j''c''} \tag{C3}$$

$$= \bar{\rho}G_{ik}\widetilde{u_k''c''} - \bar{\rho}\frac{\widetilde{\epsilon_c}}{\widetilde{c''^2}}\widetilde{u_i''c''} \tag{C4}$$

where $C_0 = 2.1$ and,

$$G_{ij} = \frac{\widetilde{\epsilon}}{\widetilde{k}}(\alpha_1\delta_{ij} + \alpha_2 b_{ij}) + H_{ijkl}\frac{\partial\widetilde{u_k}}{\partial x_l} \tag{C5}$$

$$H_{ijkl} = \beta_1\delta_{ij}\delta_{kl} + \beta_2\delta_{ik}\delta_{jl} + \beta_3\delta_{il}\delta_{jk} \tag{C6}$$

$$+ \gamma_1\delta_{ij}b_{kl} + \gamma_2\delta_{ik}b_{jl} + \gamma_3\delta_{il}b_{jk} + \gamma_4 b_{ij}\delta_{kl} + \gamma_5 b_{ik}\delta_{jl} + \gamma_6 b_{il}\delta_{jk} \tag{C7}$$

$$\alpha_1 = -\Big[\frac{1}{2} + \frac{3}{4}C_0 + b_{ii}^2(\alpha_2 + \frac{1}{3}\alpha_3) + b_{ii}^3\alpha_3 + (\beta_2 + \beta_3 + \frac{1}{3}\gamma^*)I_1 + \gamma^* I_2\Big] \tag{C8}$$

where

$$\gamma^* \equiv \gamma_2 + \gamma_3 + \gamma_5 + \gamma_6 \quad \gamma_1 = \gamma_4 = 0.0 \quad \beta_1 = -0.2$$

$$I_1 \equiv b_{ij}S_{ij} \quad S_{ij} \equiv \frac{1}{2}\frac{\widetilde{k}}{\widetilde{\epsilon}}\Big[\frac{\partial\widetilde{u_i}}{\partial x_j} + \frac{\partial\widetilde{u_j}}{\partial x_i}\Big]$$

$$I_2 \equiv b_{ij}^2 S_{ij} \quad b_{ii}^2 = b_{ij}b_{ji} \quad b' \equiv (b_{ii}^2)^{1/2} \tag{C9}$$

Table C1. Coefficients for the Haworth and Pope (HP2) model [27] and the Lagrangian (LSSG) version [70] of the SSG model by Speziale et al. [28].

	α_2	α_3	β_2	β_3	γ_2	γ_3	γ_5	γ_6
LSSG	4.0+3.4I_1	-8.85-10.2I_1	0.8-$\frac{3}{8}b'$	-0.2-$\frac{3}{8}b'$	0	0	1.2	-1.2
HP2	3.78	0	0.8	-0.2	1.04	-0.34	1.99	-0.76

Appendix D. Conversion Between Reynolds and Favre Averages

Experimental data of Goh et al. [78] measured by PIV (Particle Image Velocimetry) are based on conventional (Reynolds) averages. However, simulations for turbulent reacting flows are typically based on Favre-averaged terms. Bray et al. [6] derived a formulation of statistical description for turbulent premixed flames and linked conventionally averaged and Favre-averaged terms. Formulas adopted in the present work are as follows,

$$\widetilde{c} = \frac{\overline{c}}{1+\tau-\tau\overline{c}} \tag{D1}$$

$$\widetilde{U}_i = (1-\widetilde{c})\overline{U}_{ir} + \widetilde{c}\overline{U}_{ip} \tag{D2}$$

$$\widetilde{c''c''} = \overline{c'c'}\frac{(1+\tau\widetilde{c})^2}{1+\tau} \tag{D3}$$

$$\widetilde{u_i''c''} = \overline{u_i'c'}\frac{(1+\tau\widetilde{c})^2}{1+\tau} \tag{D4}$$

$$\begin{aligned}\widetilde{u_i''u_i''c''} &= \widetilde{c}(1-\widetilde{c})[\overline{U}_{ip}^2 - \overline{U}_{ir}^2 + 2\widetilde{U}_i(\overline{U}_{ir}-\overline{U}_{ip}) \\ &\quad + (\overline{u_{ip}'u_{ip}'} - \overline{u_{ir}'u_{ir}'})]\end{aligned} \tag{D5}$$

$$\widetilde{u_i''u_i''} = \overline{u_i'u_i'} - \widetilde{u_i''u_i''c''}\frac{\tau}{(1+\tau\widetilde{c})} + \Big(\frac{\tau\widetilde{u_i''c''}}{1+\tau\widetilde{c}}\Big)^2 \tag{D6}$$

It is noted that expansion ratio (τ) and all conventional averages including conditional averages are available from experiments [79]. Favre-averaged terms can thus be obtained from Eqs. (D1)-(D6).

Tables

Table 1. Modelled Governing Equations

Continuity

$$\frac{\partial \bar{\rho}}{\partial t} + \frac{\partial \bar{\rho}\widetilde{u_l}}{\partial x_l} = 0$$

Momentum

$$\frac{\partial \bar{\rho}\widetilde{u_i}}{\partial t} + \frac{\partial \bar{\rho}\widetilde{u_l}\widetilde{u_i}}{\partial x_l} = -\frac{\partial \bar{p}}{\partial x_i} + \frac{\partial}{\partial x_l}(\overline{\tau_{il}} - \bar{\rho}\widetilde{u_i'' u_l''})$$

Scalar

$$\frac{\partial \bar{\rho}\widetilde{c}}{\partial t} + \frac{\partial \bar{\rho}\widetilde{u_l}\widetilde{c}}{\partial x_l} = \frac{\partial}{\partial x_l}(\overline{j_l} - \bar{\rho}\widetilde{u_l'' c''}) + \bar{S}_c$$

$$\widetilde{c} < \widetilde{c}_* : \bar{S}_c = C_{R_1}\rho_u \frac{S_L}{v_K}\frac{\widetilde{\epsilon}}{\widetilde{k}}\widetilde{c}^2\Big(1-\widetilde{c}\Big); \widetilde{c} \geqslant \widetilde{c}_* : \bar{S}_c = C_{R_2}\rho_u \frac{S_L}{v_K}\frac{\widetilde{\epsilon}}{\widetilde{k}}\widetilde{c}\Big(1-\widetilde{c}\Big) \text{ where } \widetilde{c}_* = 0.03$$

$$C_{R_2} = 3.8\ (C_{R_1} = 127) \text{ for } 1\text{D cases},\ C_{R_2} = 3.0\ (C_{R_1} = 100.0) \text{ for } 2\text{D cases}$$

Reynolds stresses

$$\frac{\partial \bar{\rho}\widetilde{u_i'' u_j''}}{\partial t} + \frac{\partial \bar{\rho}\widetilde{u_l}\widetilde{u_i'' u_j''}}{\partial x_l} = \frac{\partial}{\partial x_k}\left[C_s\bar{\rho}\frac{\widetilde{k}}{\widetilde{\epsilon}}\widetilde{u_k'' u_l''}\frac{\partial \widetilde{u_i'' u_j''}}{\partial x_l}\right] + P_{ij} + \Phi_{ij} + \phi_{ij}^D + \phi_{ij}^T + \phi_{ij}^{CD} + \phi_{ij}^A - \bar{\rho}\epsilon_{ij}$$

$$P_{ij} = -\bar{\rho}\left[\widetilde{u_i'' u_l''}\frac{\partial \widetilde{u_j}}{\partial x_l} + \widetilde{u_j'' u_l''}\frac{\partial \widetilde{u_i}}{\partial x_l}\right] \quad \Phi_{ij} = -\left[\overline{u_i''}\frac{\partial \bar{p}}{\partial x_j} + \overline{u_j''}\frac{\partial \bar{p}}{\partial x_i}\right] \quad C_s = 0.22$$

$$\phi_{ij}^{CD} - \bar{\rho}\epsilon_{ij} + \phi_{ij}^A + \phi_{ij}^D + \phi_{ij}^T = \bar{\rho}G_{ik}\widetilde{u_k'' u_j''} + \bar{\rho}G_{jk}\widetilde{u_k'' u_i''} + \bar{\rho}C_0\delta_{ij}\widetilde{\epsilon} + C_{A_R}\left[\Phi_{ij} - \frac{1}{3}\delta_{ij}\Phi_{kk}\right]$$

$$+ 2\Big(\tau S_L\Big)_*{}^2\overline{S_c}\Big(\bar{c} - \frac{1}{2}\Big)\Big(1 + \beta_1\frac{\tau}{1+\tau\widetilde{c}}\Big)\Big\langle\Big(\boldsymbol{n}\cdot\boldsymbol{N_i}\Big)\Big(\boldsymbol{n}\cdot\boldsymbol{N_j}\Big)\Big\rangle\delta_{ij}$$

$$- \frac{2}{3}\delta_{ij}\frac{\partial}{\partial x_l}\left[C_p f_c\bar{\rho}\frac{\widetilde{u_k'' u_m''}u_m''}{\widetilde{\epsilon}}\frac{\partial \widetilde{U_p}}{\partial x_k}\widetilde{u_l'' u_p''} + \frac{1}{5}\bar{\rho}\widetilde{u_l'' u_n'' u_n''}\right] + 2(\tau S_L)\frac{\widetilde{u_i'' c''}}{\widetilde{c}(1-\widetilde{c})}\overline{S_c}\Big(\widetilde{c} - \frac{(1-\widetilde{c})}{(1+\tau\widetilde{c})}\Big)\Big\langle\boldsymbol{n}\cdot\boldsymbol{N_i}\Big\rangle\delta_{ij}$$

$$C_0 = 2.1, C_{A_R} = -0.30, \beta_1 = 0.42, C_p = 0.40, f_c = C_{c1}\exp(C_{c2}I), C_{c1} = 0.28, C_{c2} = 0.60, I = \sqrt{\widetilde{k}/\widetilde{U_j U_j}}$$

Scalar fluxes

$$\frac{\partial \bar{\rho}\widetilde{u_i'' c''}}{\partial t} + \frac{\partial \bar{\rho}\widetilde{u_l}\widetilde{u_i'' c''}}{\partial x_l} = \frac{\partial}{\partial x_k}\left[C_s\bar{\rho}\frac{\widetilde{k}}{\widetilde{\epsilon}}\widetilde{u_k'' u_l''}\frac{\partial \widetilde{u_i'' c''}}{\partial x_l}\right] - \left[\bar{\rho}\widetilde{u_l'' c''}\frac{\partial \widetilde{u_i}}{\partial x_l} + \bar{\rho}\widetilde{u_i'' u_l''}\frac{\partial \widetilde{c}}{\partial x_l}\right] - \overline{c''}\frac{\partial \bar{p}}{\partial x_i} - C_{A_S}\overline{c''}\frac{\partial \bar{p}}{\partial x_i}$$

$$+ \bar{\rho}G_{il}\widetilde{u_l'' c''} + \frac{\overline{S_c}}{\widetilde{c''^2}}\Big(\frac{1}{2} + A_m - C_m - \widetilde{c}\Big)\widetilde{u_i'' c''} + \Big(\tau S_L\Big)_*\overline{S_c}\Big(\bar{c} - \frac{1}{2}\Big)\Big(1 + \beta_1\frac{\tau}{1+\tau\widetilde{c}}\Big)\Big\langle\boldsymbol{n}\cdot\boldsymbol{N_i}\Big\rangle$$

$$- \frac{\partial}{\partial x_i}\left[C_p f_c\bar{\rho}\frac{\widetilde{u_k'' u_m''}u_m''}{\widetilde{\epsilon}}\frac{\partial \widetilde{U_p}}{\partial x_k}\widetilde{u_p'' c''} + \frac{1}{5}\bar{\rho}\widetilde{c'' u_n'' u_n''}\right] + \frac{\widetilde{u_i'' c''}}{\widetilde{c}(1-\widetilde{c})}\overline{S_c}\Big(\widetilde{c} - \frac{(1-\widetilde{c})}{(1+\tau\widetilde{c})}\Big)$$

$$C_{A_S} = -1/3, \beta_1 = 0.42, A_m = 0.83, C_m = 0.916, (\tau S_L)_* = \frac{\tau S_L \times (\tau S_L)_{lim}}{\tau S_L + (\tau S_L)_{lim}} \quad (\tau S_L)_{lim} = 2.5 \text{ m/s}$$

Dissipation

$$\frac{\partial \bar{\rho}\widetilde{\epsilon}}{\partial t} + \frac{\partial \bar{\rho}\widetilde{u_l}\widetilde{\epsilon}}{\partial x_l} = \frac{\partial}{\partial x_k}\left[C_{s_e}\bar{\rho}\frac{\widetilde{k}}{\widetilde{\epsilon}}\widetilde{u_k'' u_l''}\frac{\partial \widetilde{\epsilon}}{\partial x_l}\right] - C_{\epsilon_1}\bar{\rho}\frac{\widetilde{\epsilon}}{\widetilde{k}}\widetilde{u_k'' u_l''}\frac{\partial \widetilde{u_k}}{\partial x_l} - C_{\epsilon_2}\bar{\rho}\frac{\widetilde{\epsilon}}{\widetilde{k}}\widetilde{\epsilon} - C_{\epsilon_3}\frac{\widetilde{\epsilon}}{\widetilde{k}}\overline{u_l''}\frac{\partial \bar{p}}{\partial x_l}$$

$$C_{S_e} = 0.18, C_{\epsilon_1} = 1.44, C_{\epsilon_2} = 1.92, C_{\epsilon_3} = 1.44.$$

Table 2. Characteristic parameters from the DNS database [17].

	Case H	Case M	Case L
τ	6.53	4.00	1.50
S_L (m/s)	0.600	0.523	0.416
u' (m/s)	0.528	0.528	0.524
l_T(mm)	3.45	3.44	3.44

Table 3. Comparisons of thermodynamic parameters of reactants (subscript u) used in DNS and 1D RANS simulations with T temperature, P pressure, μ dynamic viscosity, C_p specific heat capacity at constant pressure and γ ratio of heat capacities.

	T_u(K)	P_u(MPa)	ρ_u(kg/m^3)	μ_u(Pa · s)	C_p(J/kg · K)	γ
DNS	300	0.1	0.933	1.77×10^{-5}	1.25×10^3	1.4
RANS	300	0.1	0.933	1.65×10^{-5}	1.25×10^3	1.4

Table 4. Comparison of computed turbulent burning velocities obtained with the model parameters listed in Table 3.

Method	H Flame	M Flame	L Flame
DNS [71]	1.12 m/s	0.99 m/s	0.74 m/s
Quasi-1D simulations	1.30 m/s	0.98 m/s	0.80 m/s

Table 5. Flame parameters from calculations using detailed chemistry [80] with ϕ the equivalence ratio, S_L the unstrained laminar burning velocity and τ the expansion ratio.

Fuel	ϕ	S_L(m/s)	τ
CH_4	0.9	0.325	5.720
CH_4	0.8	0.262	5.406

Table 6. Case configurations for the H flame [17, 18] defined in Table 2.

Case No.	$\overline{p' \frac{\partial u_i''}{\partial x_i}}$ and $\left(\overline{p' \frac{\partial c''}{\partial x_i}}\right)_f$	β_1	$\left(\overline{\frac{\partial p' u_i''}{\partial x_i}}\right)_f$ and $\left(\overline{\frac{\partial p' c''}{\partial x_i}}\right)_f$
1	–	–	–
2	Eqs. (24) and (25)	0.00	Eqs. (29) and (30)
3	Eqs. (24) and (25)	0.42	Eqs. (29) and (30)

Figures

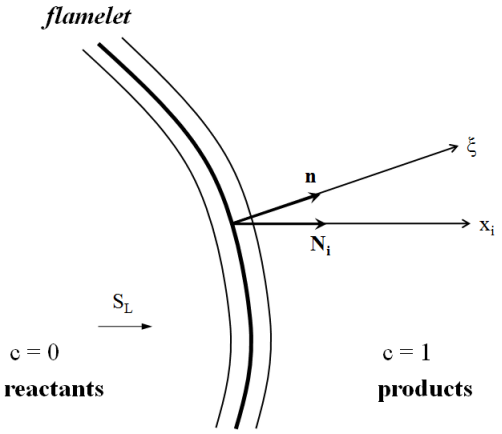


Figure 1. Definition of unit vectors ($\boldsymbol{n}$ and $\boldsymbol{N_i}$)

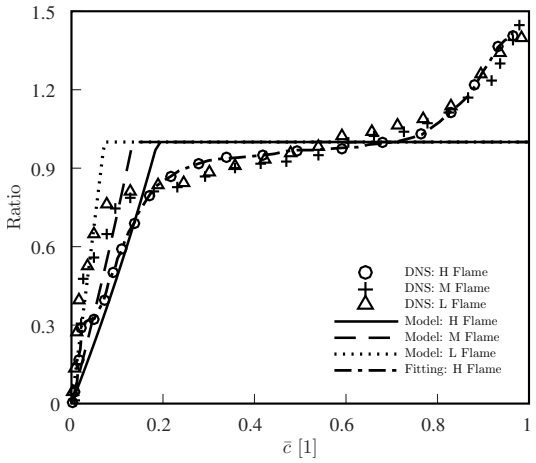
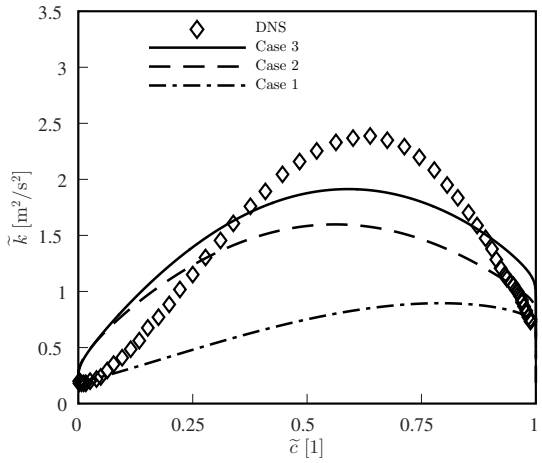
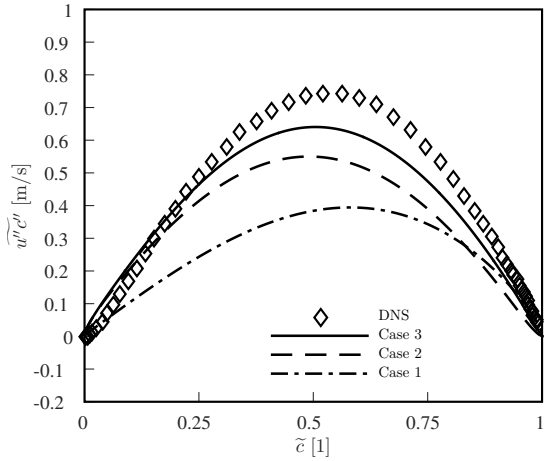


Figure 2. The ratio of $\overline{S_c}/(\rho_u S_L \Sigma)$ [71] and the current bridged expression normalised by the relation of Lindstedt and Váos [31]. A curve fit of the form $\bar{c} \cdot [8.0(\bar{c} - 0.80)^2 + 1.3]$ to the data arising from the DNS simulation of Flame H is also shown.

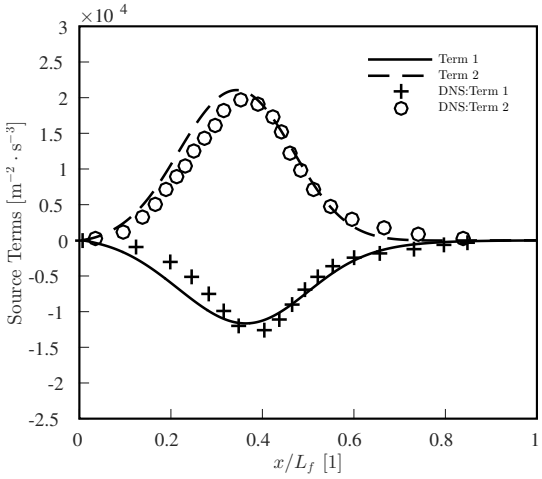


(a)

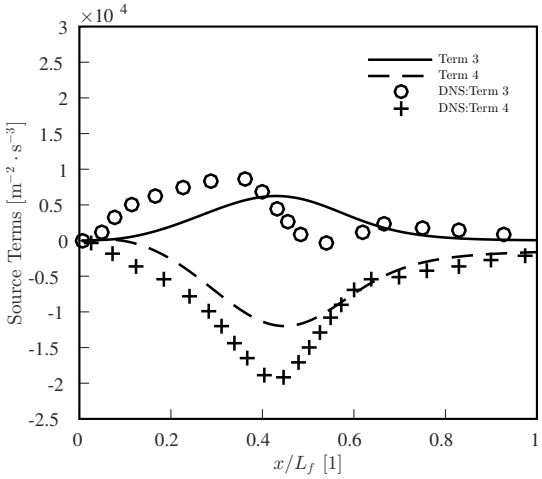


(b)

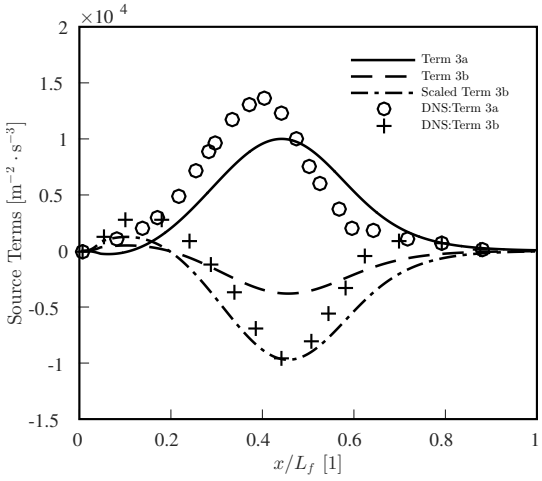
Figure 3. Effects of dilatation/scrambling models as outlined in Table 6 on (a) predicted turbulent kinetic energy and (b) scalar flux for H flame (see Table 2).



(a)

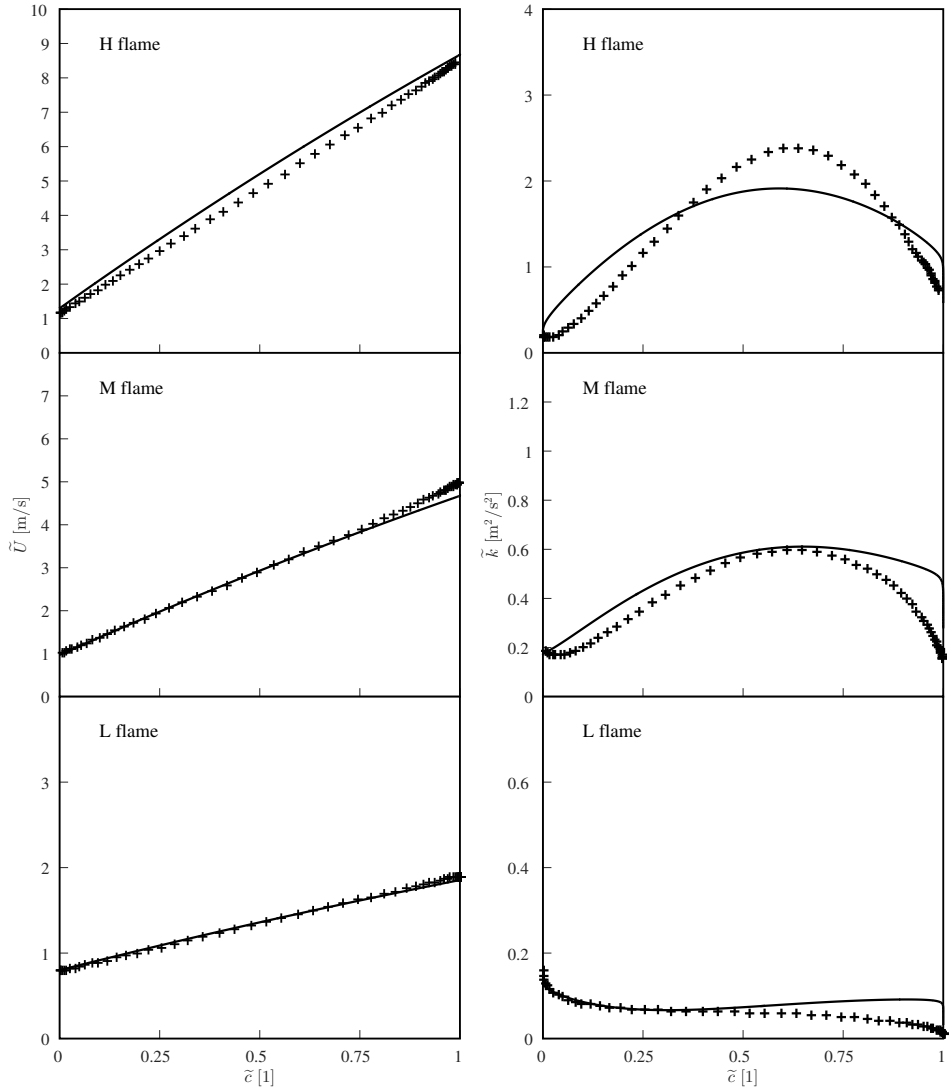


(b)



(c)

Figure 4. Source terms for the turbulent kinetic energy ($\widetilde{k}$) for H flame (see Table 2); Term 1: $-\frac{\overline{\rho u_i'' u_k''}}{\bar{\rho}} \frac{\partial \widetilde{u_i}}{\partial x_k}$; Term 2: $-\frac{\overline{u_i''}}{\bar{\rho}} \frac{\partial \bar{p}}{\partial x_i}$; Term 3: $-\frac{1}{\bar{\rho}} \overline{u_i'' \frac{\partial p'}{\partial x_i}}$; Term 3a: $\frac{1}{\bar{\rho}} \overline{p' \frac{\partial u_i''}{\partial x_i}}$; Term 3b: $-\frac{1}{\bar{\rho}} \frac{\partial \overline{p' u_i''}}{\partial x_i}$: Term 4: $\frac{1}{\bar{\rho}} \overline{u_i'' \frac{\partial \tau_{ik}}{\partial x_k}}$ (see Eq. (43)).



(a) (b)

Figure 5. Comparisons of (a) predicted mean velocity and (b) turbulent kinetic energy with DNS data under different expansion ratios (conditions as shown in Table 2).

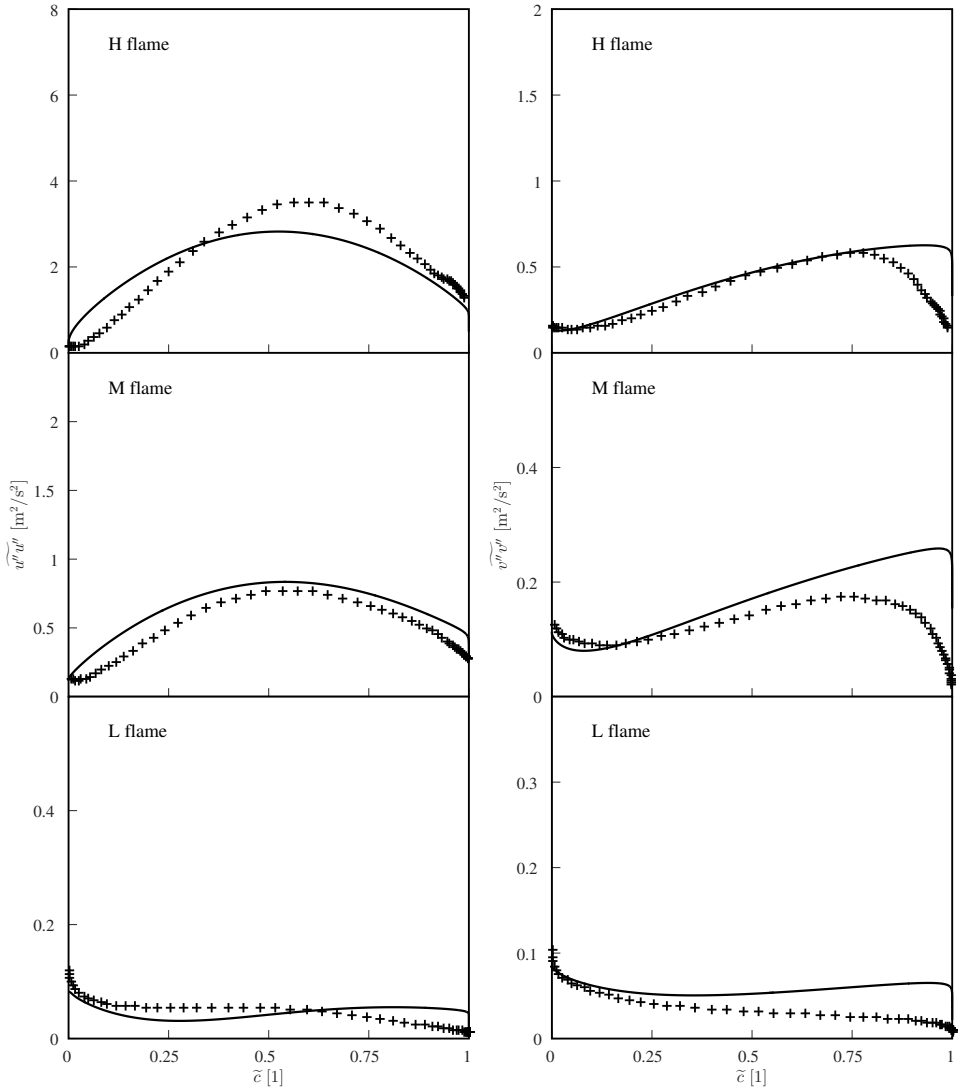


Figure 6. Comparisons of predicted (a) axial and (b) radial Reynolds stresses with DNS data under different expansion ratios (conditions as shown in Table 2).

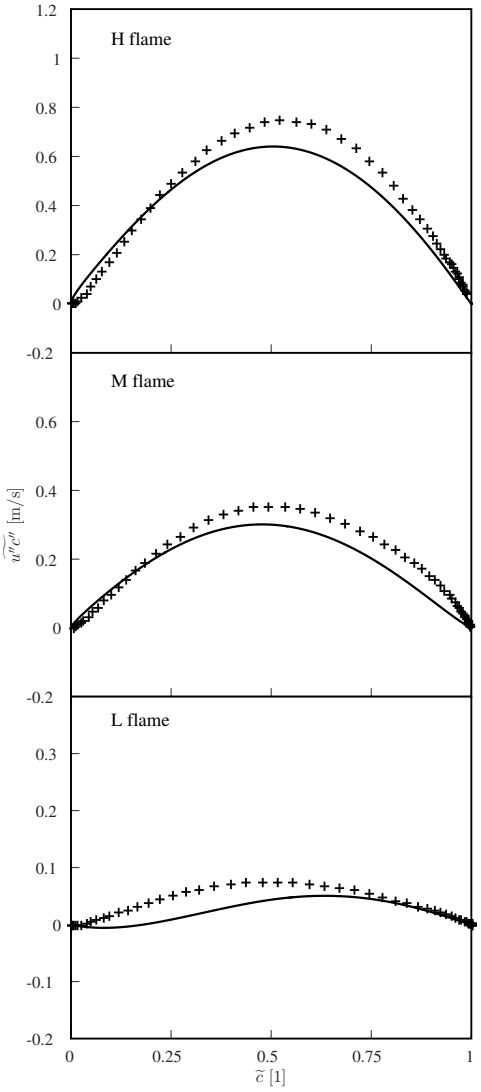
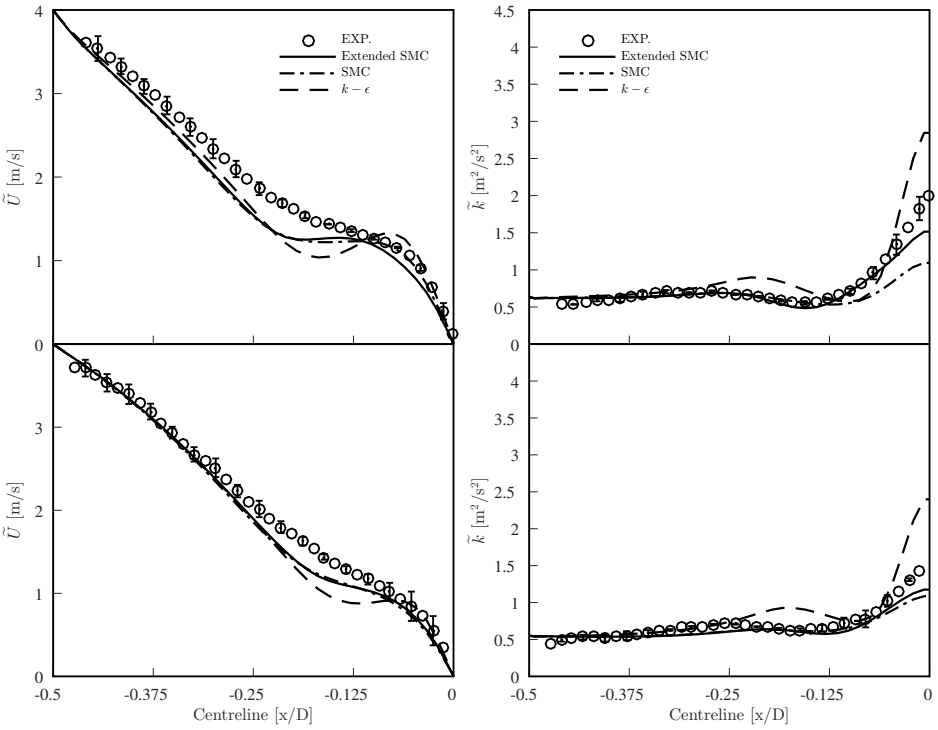
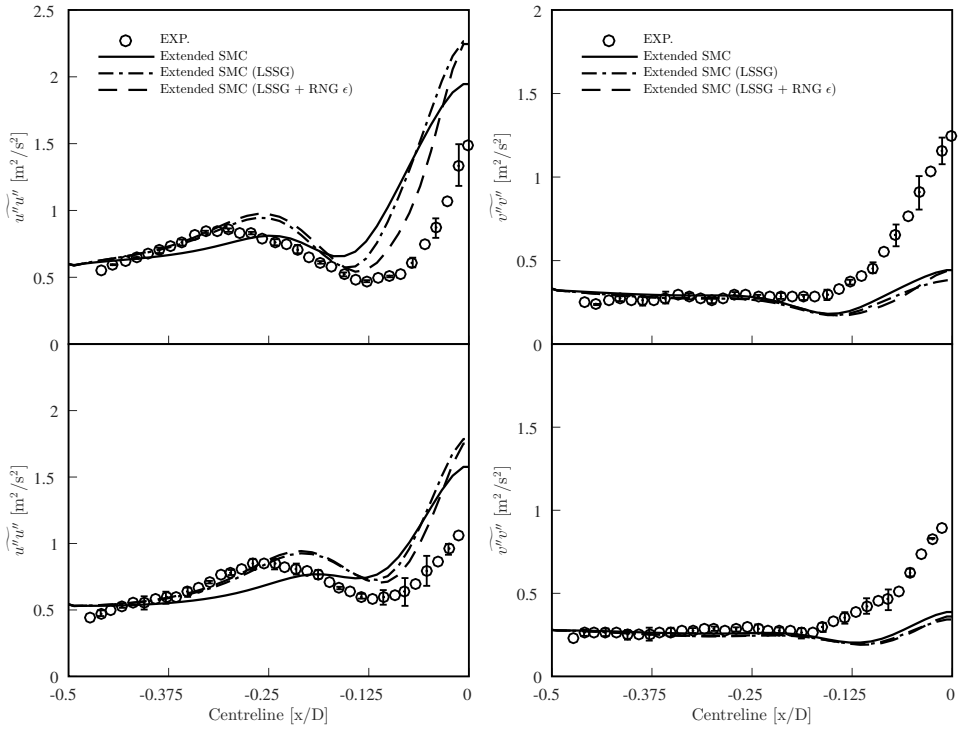


Figure 7. Comparisons of predicted turbulent scalar flux with DNS data under different expansion ratios (conditions as shown in Table 2).



(a) (b)

Figure 8. Predicted and (a) measured mean velocity and (b) turbulent kinetic energy along the centreline in opposed jet flames. Top row: $\phi = 0.90$. Bottom row: $\phi = 0.80$ (conditions as shown in Table 5).



(a) (b)

Figure 9. Predicted and measured (a) axial and (b) radial Reynolds stresses along the centreline in opposed jet flames. Top row: $\phi = 0.90$. Bottom row: $\phi = 0.80$ (conditions as shown in Table 5).

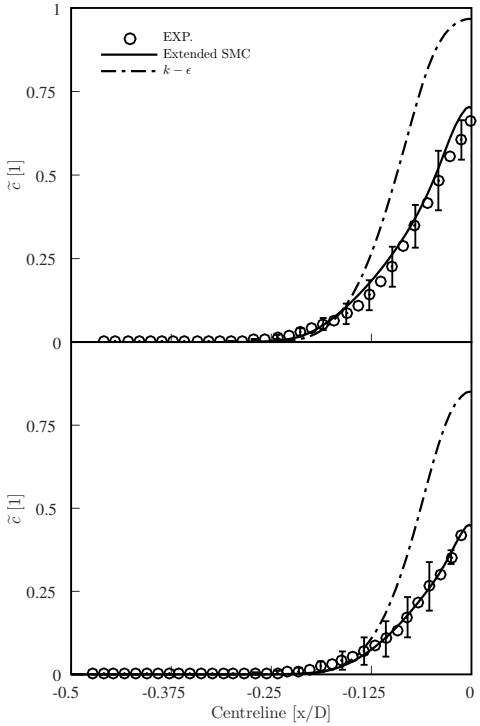
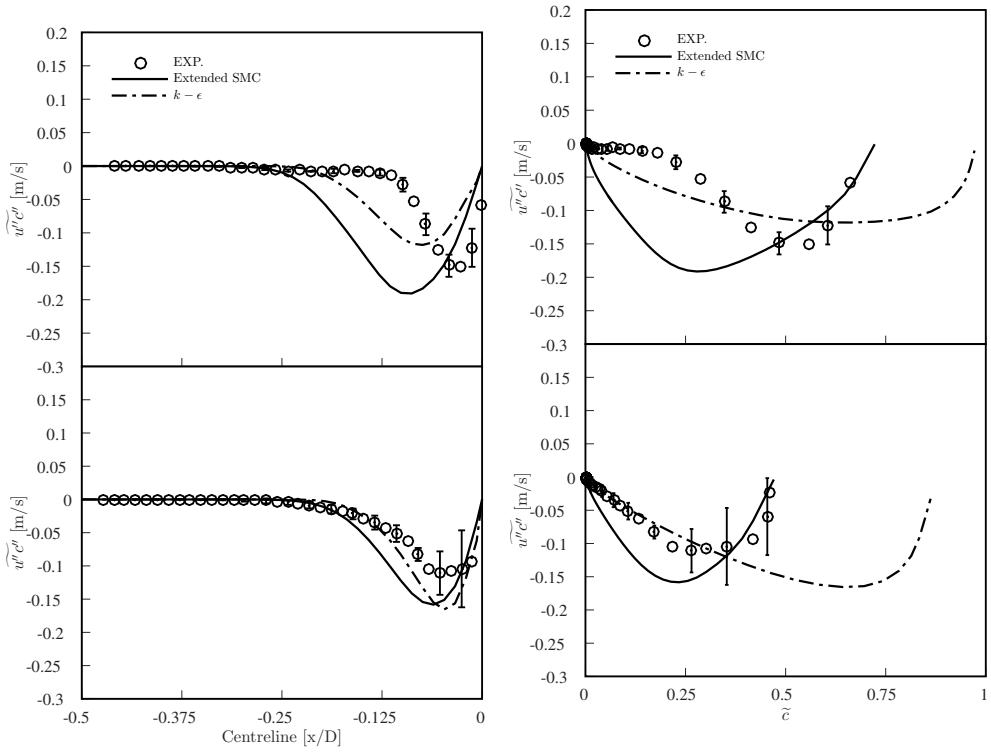


Figure 10. Predicted and measured reaction progress variable along the centreline in opposed jet flames. Top row: $\phi = 0.90$. Bottom row: $\phi = 0.80$ (conditions as shown in Table 5).



(a) (b)

Figure 11. Predicted and measured turbulent scalar flux in (a) physical space and in (b) reaction progress variable ($\widetilde{c}$) space. Top row: $\phi = 0.90$. Bottom row: $\phi = 0.80$ (conditions as shown in Table 5).